

Philips Technical Review

DEALING WITH TECHNICAL PROBLEMS
RELATING TO THE PRODUCTS, PROCESSES AND INVESTIGATIONS OF
THE PHILIPS INDUSTRIES

EDITED BY THE RESEARCH LABORATORY OF N.V. PHILIPS' GLOEILAMPENFABRIEKEN, EINDHOVEN, NETHERLANDS

A UNIVERSAL APPARATUS FOR X-RAY THERAPY WITH MOVING FIELD IRRADIATION

by H. VERSE *).

621.386.1:615.849

Deep therapy with X-rays, that is, the treatment of tumours sited deep within the body, is one of the most difficult and least rewarding branches of medical practice. Attempts are continually being made to better the conditions in this phase of therapeutics by the application of new technical aids. The apparatus for moving field irradiation described in this article constitutes a further advance in this direction. Of course, the moving field irradiation technique, which with this unit is of quite general application, is by no means capable of effecting a cure in every case. Experience has shown however that with this technique the complicating subsidiary effects of the treatment can be largely eliminated, and that a higher percentage of cures in many kinds of cases can be obtained.

Deep therapy and moving field irradiation

A problem long associated with the X-ray treatment of lesions (tumours) sited deep within the body is that of administering a suitable dose of radiation to the morbid tissues without damaging the surrounding healthy tissues, especially those near the surface of the body. Considered superficially, this is apparently impossible when the irradiation is from an outside source; the dosage rate is always higher on the skin than in the lesion, owing to the usual decrease in radiation intensity with the square of the distance, and to the roughly exponential attenuation of the radiation with increasing depth of penetration. The ratio of the lesion dose to the skin dose can be increased considerably in two ways: firstly by decreasing the relative differences in distance by using a relatively long source-skin distance, or by "compressing" the patient; secondly by employing hard X-rays (high tube voltage and heavy filter) and so obtaining a more gradual decrease in the dose with increasing depth. However, the percentage values of the lesion dose/skin dose ratio, i.e. the *relative depth dose*, obtainable in this way do not exceed about 40% (when the lesion is 10 cm beneath the skin). Hence the success of the treatment depends entirely on how

far the radiation *tolerance* of the healthy tissue exceeds that of the morbid tissue. Even if parts of the body outside the lesion suffer no permanent injury, the patient generally takes quite a long time to recover from the heavy load imposed on these parts.

The use of extremely hard radiation (equivalent tube voltage of several million volts) is more favourable from a physical point of view. Owing to the directional effect of the secondary X-rays and electrons generated within the body by the hard rays, a *dosage maximum* is produced below the surface of the body. The dosage maximum can be made to coincide with the site of the lesion.

There is another — long known and inherently simple — way of avoiding the above problem, that is, by irradiating the lesion from several directions (using normal tube voltages of 200 to 250 kV) and so rendering the skin dose innocuous. Multiple field irradiation, cross-fire irradiation and moving field irradiation¹⁾ (with a moving tube) function in this way.

The continual progress made during the last decade in the development of X-ray tubes and high tension shields, especially with regard to their

¹⁾ See: G. F. Haenisch and H. Holthusen, *Einführung in die Röntgenologie*, G. Thieme, Stuttgart 1951.

*) C. H. F. Müller A. G., Hamburg-Fuhlsbüttel.

decrease in size and weight, has led to an entirely new approach to the mechanical problem of moving field irradiation, under far more favourable conditions than before. In particular, these developments have widened the possibilities for a fuller exploitation of the advantages associated with a moving tube. With this in view, the X-ray works of C.H.F. Müller in Hamburg have produced a new

of these features is governed by medical requirements and by constructional limitations. The TU 1 is based on a *horizontal* positioning of the patient (see fig. 1) and a movement of the tube over a circular arc about his horizontal axis³⁾. The design of this apparatus was considerably influenced, however by the fact that irradiation over a single circular arc is in some cases not sufficient.

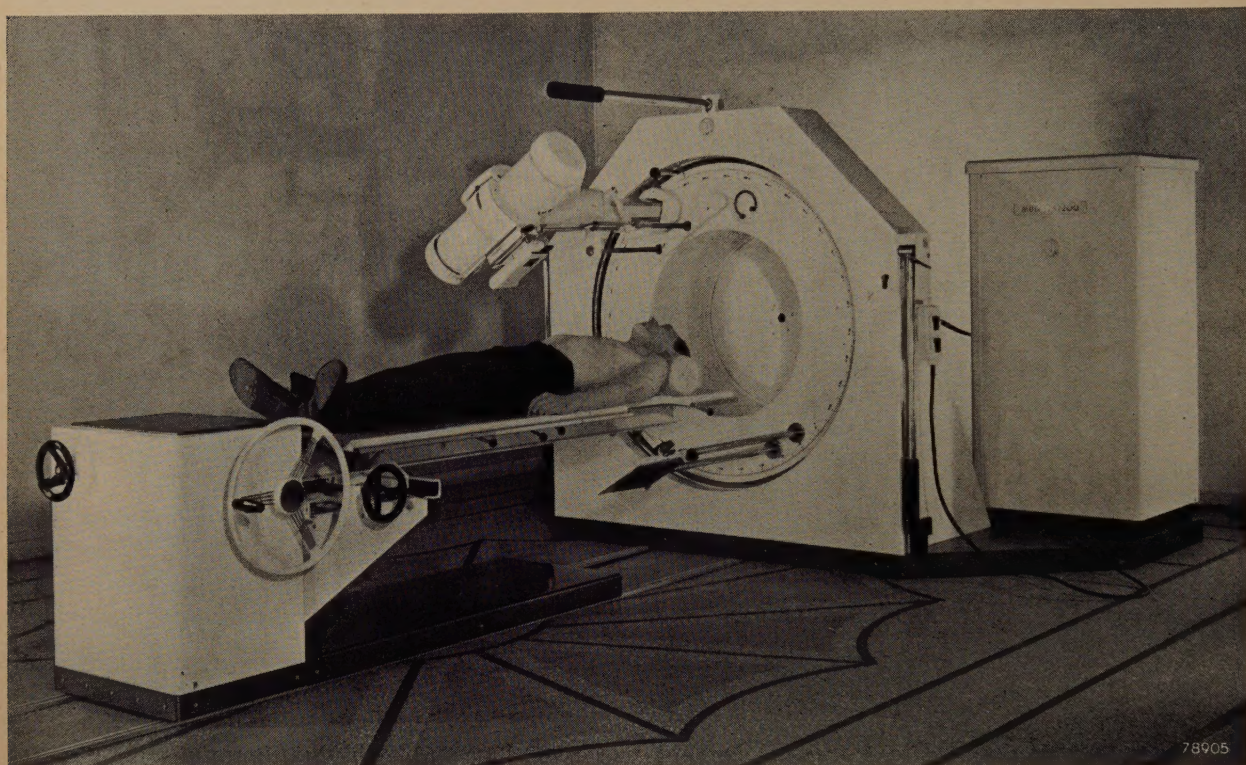


Fig. 1. View of the Müller TU 1 equipment for moving field X-ray irradiation. The treatment-table, running on rails, is seen on the left, the mounting for the X-ray tube and shield at the centre, and the H.T. generator (Müller RT 200) for the X-ray tube on the right of the photograph. The control desk is placed behind a lead glass screen in an adjoining room.

constructional solution to the problem of moving field irradiation, namely, the TU 1 apparatus²⁾ illustrated in fig. 1, which will now be described.

Principles of the design

Briefly, the principle of moving tube irradiation is that during irradiation the X-ray tube is moved in a specific path around the body of the patient, so that, while the cone of X-rays is always directed at the tumour, the region of entry of the rays moves continually from one area of skin to another.

There are many possibilities as regards the shape of the path and the geometrical details; the choice

This is borne out by the following observations concerning the dosage distribution in the body during moving tube irradiation⁴⁾.

²⁾ H. Verse, Einige gerätetechnische Überlegungen zur Röntgenbewegungsbestrahlung, Fortschritte Röntgenstrahlen u. Röntgenpraxis 77, 362-367, 1952.

³⁾ According to a method evolved elsewhere, the patient is irradiated in a sitting position (R. Du Mesnil de Rochemont and H. Fiebelkorn, Strahlentherapie 88, 198-205, 1952). The X-ray tube is then fixed and the patient is rotated about a vertical axis with the aid of a revolving chair during irradiation. We prefer a horizontal attitude of the patient in view of the combination of rotational and traversing movements used. Indeed, to produce the desired concentration of X-rays at precisely the correct point in the body, such a combination of movements can hardly be achieved in any other way than with the patient horizontal and completely immobilized. Moreover, this position is of course more suitable for patients who are gravely ill.

⁴⁾ The data here employed are derived mainly from the investigations of Howard Nielsen; see his book: Rotations Bestraaling, Munksgaard, Copenhagen 1948, and the publication: Rotary Irradiation, Acta Radiol. 37, 318-328, 1952.

Fig. 2a shows the computed dosage distribution in a cylindrical paraffin-wax phantom 30 cm in diameter irradiated with a stationary tube focus. If no filter is placed in the path of radiation, the dosage at the centre of the cylindrical body, that is, 15 cm beneath the "skin", is only 11% of the surface dose⁵). When the focus is moved so that it describes a full circle about the phantom, "isodose" curves of radial

extremely sensitive organs which must not come within range of the X-ray beam, and not useful if the rays in passing through a particular angular region must penetrate heavy bones and thus undergo considerable attenuation before reaching the tumour. The isodoses produced in the above phantom when the tube movement is restricted to particular arcs of the circle are shown in figures

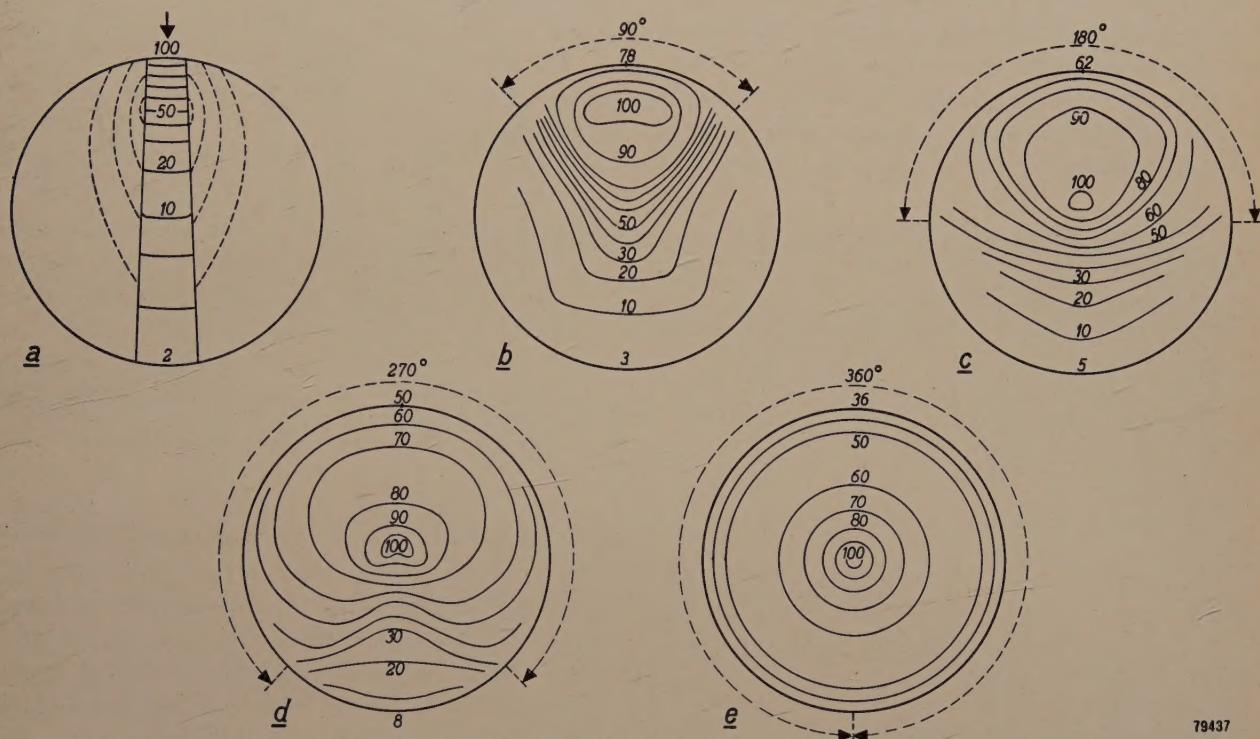


Fig. 2. Isodoses in a cylindrical phantom of paraffin wax 30 cm in diameter, when a field 5 cm wide and 15 cm along the axis of the cylinder is irradiated at a focus-lesion distance of 50 cm, by radiation of half-value thickness 0.7 mm Cu (reproduced from page 47 of the book by H. Nielsen referred to in note⁴).

a) Stationary tube irradiation. The envelope of scattered radiation around the direct X-ray beam is indicated by dotted lines. The lesion dose is 11% of the surface dose.

b) Rotation of X-ray tube through an angle of 90° about the axis of the cylinder. The dosage maximum (100%) is now within the body.

c) Angle of rotation 180°.

d) Angle of rotation 270°.

e) Angle of rotation 360°. The isodoses here become concentric circles. The dosage maximum is at the axis of the cylinder; the skin dose is everywhere only 36% of the dosage maximum.

symmetry are obtained (fig. 2e). The centre dose is then 280% of that at every point on the surface of the cylinder; this demonstrates the great advantage of moving tube, compared with stationary tube irradiation. In some cases, however, it is neither feasible nor useful to move the tube through the whole 360° angle about the patient: not feasible if a particular region of this angular field includes

2b, c and d. The relative dosage distributions along the diameter of the phantom which passes through the dosage maximum are shown in fig. 3 for all these cases. It will be seen that the relative depth dose decreases appreciably as the angle of rotation is made smaller; instead of 280%, it is only 130% at the dosage maximum when the angle of rotation is 90°. (The patient is of course so positioned that the dosage maximum lies in the tumour. It may well happen that the disposition of the tumour and the portion of the skin used as a port of entry are such that the pivoting point of the required circular tube movement is not on the axis of the

⁵) The relative depth dose mentioned at the beginning of this article, viz. 40% at a depth of 10 cm, applies to the irradiation of a large field with the aid of a heavy filter, this being the method usually employed in normal deep therapy to increase the depth dose; such filtration naturally necessitates the use of a far more powerful X-ray tube.

patient. As a consequence the dosage distribution may differ considerably from those of fig. 2. This does not affect the qualitative validity of the argument however.)

Thorough investigations have demonstrated⁶⁾ that it is impossible to improve matters either by increasing the focus-skin distance or by using harder rays (employing a filter). A very considerable relative depth dose, however, can still be obtained with a comparatively small angular rotation, if the region of entry of the rays is made to describe a number of parallel bands on the skin of the patient, the cone of X-rays being always directed at the same point in the tumour throughout

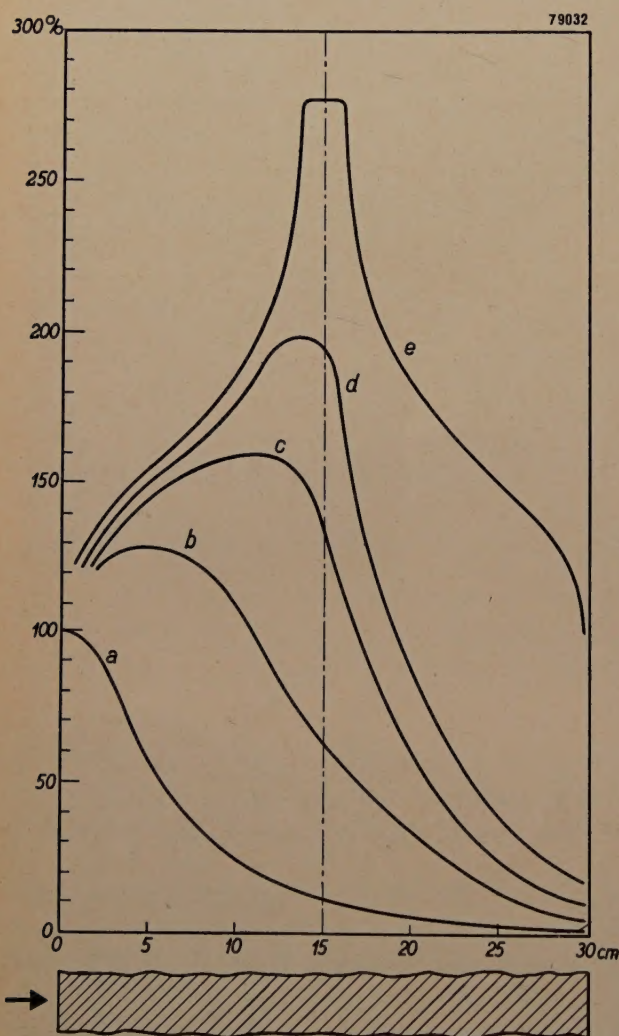


Fig. 3. Dosage distribution along the diameter running through the dosage maximum, of the cylindrical paraffin wax phantom shown in figures 2a to 2e inclusive. The arrow indicates the direction of the X-rays.

⁶⁾ R. Du Mesnil de Rochemont, Die Dosierungsgrundlagen der Rotationsbestrahlung, *Strahlentherapie* **60**, 648-674, 1937. M. Nakaidzumi and A. Miyakawa, Über die räumliche Dosisverteilung der Röntgenstrahlen bei der Rotationsbestrahlung, *Strahlentherapie* **66**, 583-592, 1939.

the process (see fig. 4). This is termed convergent irradiation. To accomplish it the tube must of course perform in addition another kind of movement such that the rotation about the patient takes place in a succession of different planes.

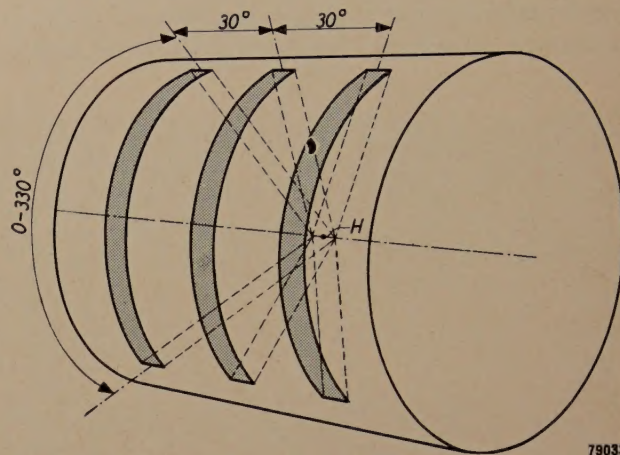


Fig. 4. Convergent irradiation of the cylindrical phantom. The port of entry of the X-ray beam describes parallel bands on the surface of the skin. The cone of rays remains always directed at the lesion *H*.

Such a spatial movement can be obtained in several ways; in the TU 1 it is done by imparting to the X-ray tube a traverse at right-angles to the rotation, which can be controlled independently of the latter. The advantages associated with the above solution and the manner of its application in the practical design will become apparent from the description of the apparatus given below.

Design of the irradiation apparatus

The X-ray generator used in the irradiation apparatus TU 1 is the standard Müller "RT 200" deep therapy unit, the X-ray tube of which is housed in an oil-filled shield. The Philips "250/25" deep therapy unit can be used as an alternative.

Rotational movement

The irradiation apparatus comprises a vertical disc in a fixed frame, mounted so that the disc can be rotated about its axis by an electric motor (fig. 5). Mounted near the periphery of the disc is a horizontal arm, to which the X-ray tube is attached in such a way that the X-ray beam emitted is directed towards the axis of the disc. The high tension cables and the oil ducts of the cooling system pass through the (hollow) arm to the shield of the X-ray tube. Since the tubes of both the Müller RT 200 and the Philips 250/25 units mentioned above use a D.C. voltage supply (maximum tube voltages 200 and 250 kV respectively), relatively thin, flexible H.T.

cables are employed; hence there are no difficulties when the tube is moved.

To enable the patient to be so positioned in the cone of rays that the lesion is at the correct place (that is, in the region of the dosage maximum), the apparatus is equipped with a special treatment-table which runs on rails set in the floor parallel to the axis of the rotating disc; the table top, on which the patient lies, can be adjusted vertically and laterally.

The diameter of the circular path described by the focus of the X-ray tube is 1 metre; hence the focus is (at most) 50 cm from the lesion and, on an average, 30 to 40 cm from the skin of the patient.

In order that the tube shall not strike the table during the rotational movement, the table top is divided into several interchangeable plates one of which, to be placed in the appropriate position, is cut away to allow the tube to pass (see fig. 1).

Two end contacts (fig. 5, E_1 , E_2), which can be positioned round the rotary disc, are used to vary the angle of rotation; as soon as either of these contacts touches a corresponding fixed contact on the frame, the direction of rotation of the electric motor driving the disc is reversed. The maximum angular range is 330° ; the angle of 30° not covered includes the heavy iron table girder used to ensure perfect positional stability of the patient.

The rotational movement takes place at a rate of 6° per second.

Traversing movement

The traverse of the X-ray tube is achieved by a movement of the arm (T in fig. 5) parallel to the axis of the disc in a bush (B). This movement is

actuated by a second electric motor. Unlike the rotational drive which is mounted on the fixed frame of the apparatus and actuates the disc through a simple chain transmission, the traversing drive is mounted on the rear face of the rotary disc (fig. 6) and is connected electrically via a flexible cable to the control desk from which the movement is controlled. To produce the traversing movement of the X-ray tube, a screwed collet mounted in bearings on the disc, and driven by the motor, propels a threaded shaft attached to the tube shield. At the same time another threaded shaft, moving in the same direction as the first but more slowly, acts upon a lever mechanism which changes the position

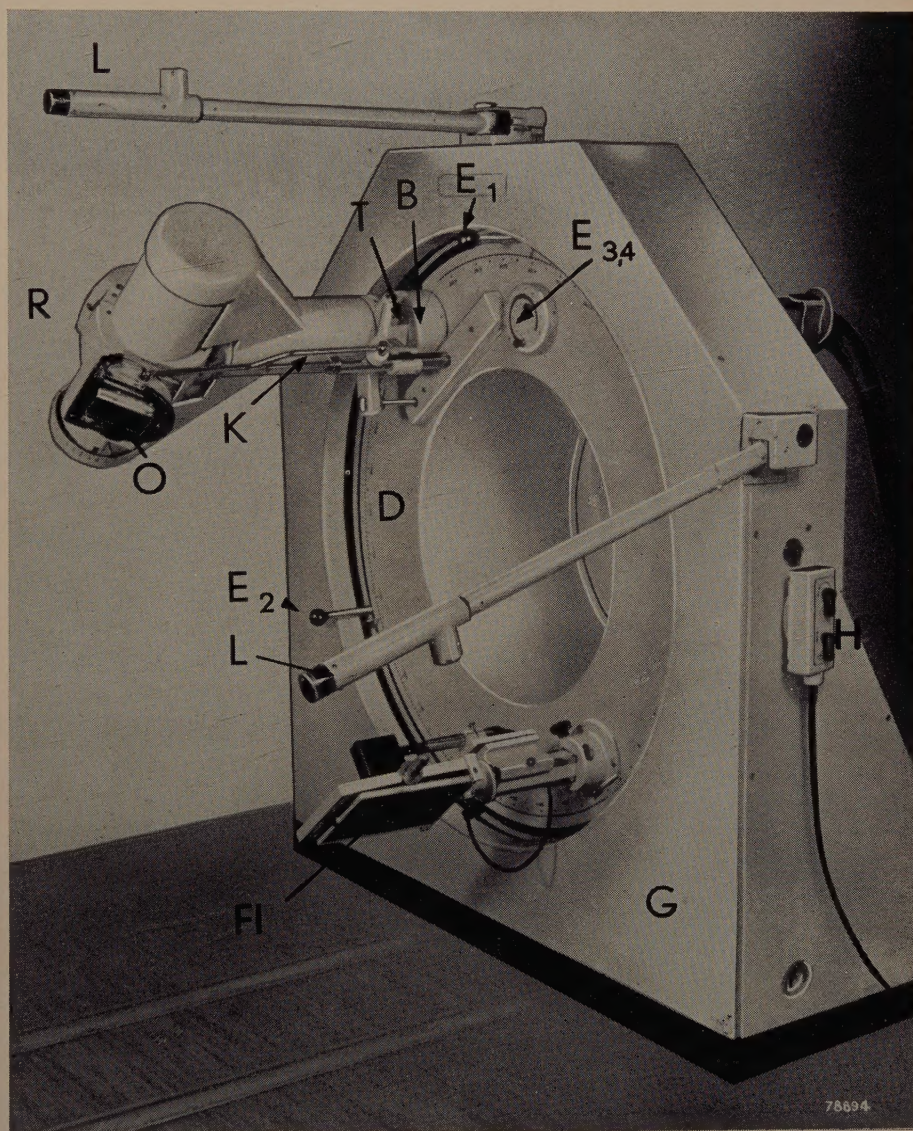


Fig. 5. Mounting for the X-ray tube. G fixed frame, D rotary disc in peripheral roller-bearing on frame, T arm carrying X-ray tube, R X-ray tube with shield and beam aperture O, K coupling rod, B bush in which arm T moves. E_1 , E_2 end contacts for rotation, E_3 , E_4 adjusting knobs for end contacts of traverse, H hand switch, F1 fluorescent screen, L two of the sources of the light beams described later. (The arrangement of the beam aperture of the apparatus shown in fig. 1 differs in some respects from that of the latest model shown here.)

of the beam aperture in the tube shield (see fig. 5 and fig. 7). The pitches of the two threads are such that their relative speeds maintain the projected cone of X-rays always directed at a given point on the axis of the disc.

The range of traverse is controlled with the aid of two end contacts, these being adjusted by means of two knobs attached to the front face of the disc (see fig. 8, which also shows other features of the design). The maximum traverse obtainable is 60 cm; this requires a corresponding rotation of the beam aperture of the tube through an angle of 60° . To treat an elongated, say, a more or less cylindrical lesion, different sections of which are to be exposed successively to rotational irradiation, the coupling rod can be removed from the lever mechanism; the X-ray beam then remains aligned in the same direction throughout the traversing movement of the tube.

This rod is likewise uncoupled when the apparatus is to be used for stationary tube irradiation (sometimes combined with compression, which is of course neither practicable nor necessary in the case of rotational irradiation). When uncoupled, the direction of the beam can be adjusted through an arc of 120° .

The normal speed of the traverse is $2/3$ cm per second; hence the tube takes 90 seconds to travel from one end of the traverse to the other.

Apart from convergent irradiation along parallel bands, the TU 1 apparatus can be used for irradiation

of another kind, which may be termed *oscillatory convergent irradiation*⁷⁾. In this process, the to-and-fro rotational movement of the tube takes place *simultaneously* with a gradual traversing

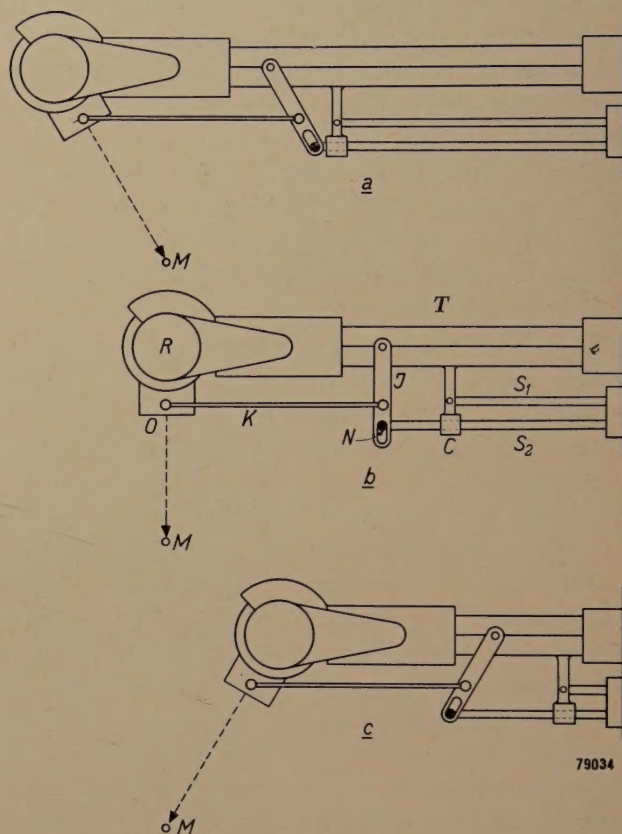


Fig. 7. Mechanism for aligning X-ray beam during traversing movement of X-ray tube R. The screwed shaft S_1 (here shown slightly displaced for clarity) is connected to carrier arm T and actuates the traverse. The threaded shaft S_2 , which moves in slide bearing C and is moved more slowly but in the same direction as S_1 , governs the position of lever J through a pin N. This lever (via the coupling rod K) moves the beam aperture O in the tube-shield through an angle (here shown in the centre and in the two extreme positions of the traversing movement, a, b, c). The central ray of the beam is thus always maintained in alignment with a fixed point M, unless coupling rod K is removed.

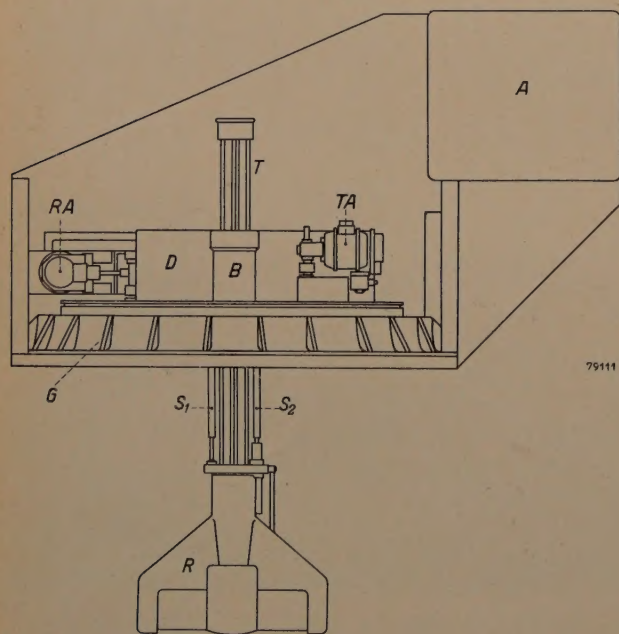


Fig. 6. Top view of main frame and X-ray tube mount with cover plates removed, G fixed frame, mounted on the same base as the H.T. generator A. RA motor unit for rotation, TA motor unit for traverse, mounted on rotary disc. S_1 , S_2 threaded shafts, other letters as in fig. 5.

movement at $1/6$ of the normal speed referred to in the above; hence the port of entry of the X-rays describes on the skin a zig-zag pattern, as shown in fig. 9. It is seen that by virtue of this gradual traverse the coverage is almost completely uniform over the entire area of skin available for the entry of X-rays. Hence this method of irradiation is particularly valuable as a means of effecting adequate distribution of the total skin dose, even in cases where, for medical reasons, the angular range of the rotation is

⁷⁾ H. Wichmann, Physikalisch-technische Bemerkungen zur Bewegungsbestrahlung, Röntgenstrahlen — Geschichte u. Gegenwart (published by C. H. F. Müller A. G.) 3, 72-79, 1953.

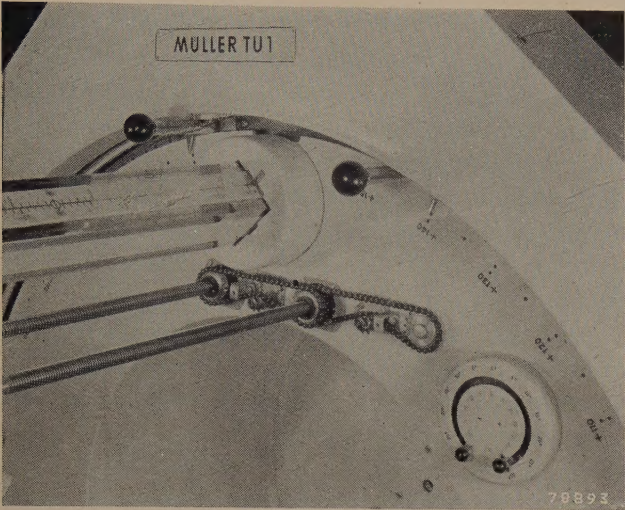


Fig. 8. Close-up of part of the rotary disc. The arm carrying the X-ray tube is seen on the left; beneath it are the two screwed collets, mounted in bearings on the disc and driven by a chain transmission, and the two threaded shafts. The two end contacts for the rotation are seen at the top, and the adjusting knobs for the traverse end contacts in the bottom right-hand corner.

restricted. If the full traversing range of 60 cm is used, the time required for complete irradiation by this method is 9 min. The dose accumulated in this period is sufficient for most cases occurring in practical X-ray therapy.

Preparations and procedure for an irradiation treatment

Positioning of the patient

The first task in preparing for the treatment is to position the patient correctly, so that the lesion (or other anatomically defined site within the body) will be at the pivoting point of the tube movement. Since this pivoting point is on the axis of the rota-

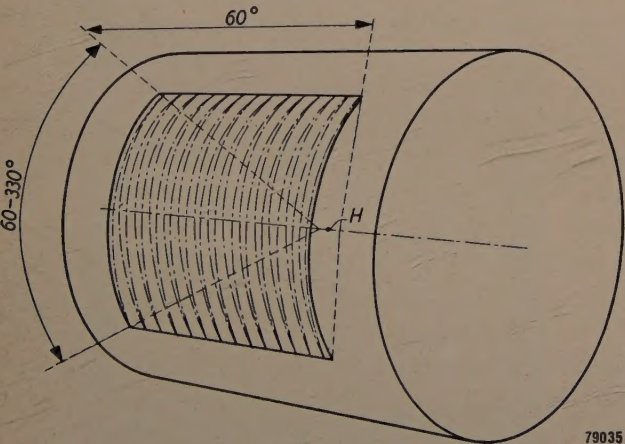


Fig. 9. Zig-zag pattern described by the port of entry of therapies on the skin of a patient undergoing oscillatory convergent irradiation. The beam is maintained in constant alignment with point H.

ting disc and is thus fixed in relation to the frame of the apparatus (it is here assumed that the coupling rod K of the lever mechanism shown in fig. 7 is in position), it can be indicated in space with the aid of a system of light beams, fixed in relation to the frame. The light-beams are provided by three light sources carried by hinged arms attached to the frame. A fourth light beam coinciding exactly with the axis of rotation, is produced by a projector at the centre of the rotating disc (fig. 10). By moving the table with the patient upon it towards or away from the disc, and adjusting the table top vertically and laterally, all these light-beams are brought to bear upon marks previously made on the skin of the patient. Correct positioning of the patient is thus ensured. A fifth light source can be mounted on the beam aperture of the X-ray tube to supply a light-

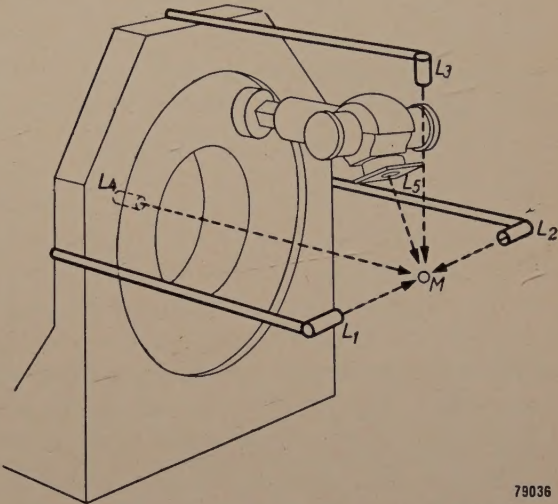


Fig. 10. Method of positioning the patient with the aid of light-beams L_1 - L_4 . A light source fitted to the beam aperture of the X-ray tube produces the light beam L_5 , which coincides with the central ray of the X-ray beam subsequently emitted. The lesion (or other specific point in the body of the patient) should be positioned at the point of intersection M of all these light beams.

beam to coincide with the central ray of the X-ray cone. Provided that the patient is correctly aligned, this light beam will always point exactly at the lesion. The three arms referred to above are provided with safety switches which, in the event of excessive deformation of any one of them, switch off all the light sources and thus prevent incorrect positioning of the patient.

The position of the patient can be checked immediately before irradiation with the aid of a small fluorescent screen attached to the rotating disc at a point directly opposite the X-ray tube. Provision for fluoroscopic examination while the beam is vertical (frequently desirable in the case

of a recumbent patient) is made by placing the iron supporting girder off-centre beneath the table, as shown in *fig. 11*. This diagram also shows the different margins of adjustment allowed for positioning the patient. To give as much clearance as possible for moving the patient along the axis of rotation, the centre portion of the rotating disc is deeply recessed (see figures 1 and 5).

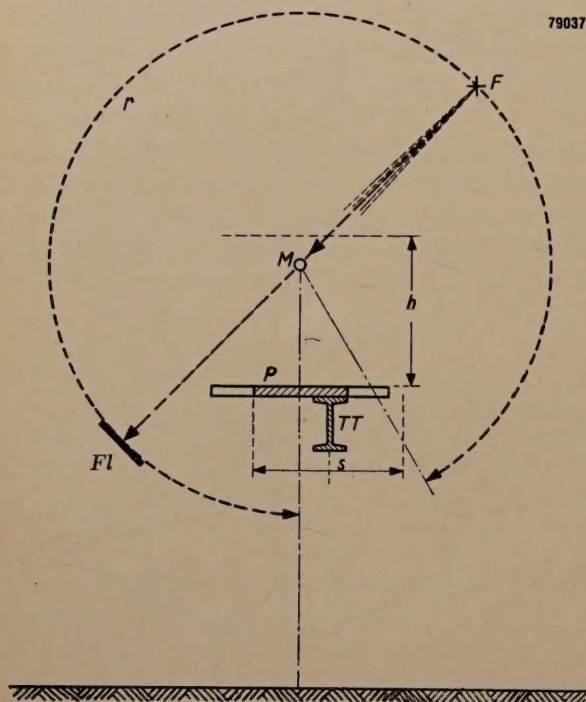


Fig. 11. The top plate P of the treatment-table can be moved vertically through a distance h and laterally over a distance s . F is the focus of the X-ray tube and Fl the fluorescent screen opposite the tube, with the aid of which the patient can be screen-tested in any position within the angular range r of the rotational movement. The iron girder TT of the table is placed off-centre to permit the use of the fluorescent screen whilst the X-ray beam is vertical.

Control and limitation of the movement

Since the apparatus is equipped with two separate motor units for the rotational and traversing movements, both of which can be controlled independently through a system of relays, a great diversity of movements can be made to take place automatically. To ensure the utmost simplicity and clarity in operation, only three of the many possibilities have been selected; these correspond to the methods of stationary tube irradiation, rotational irradiation and oscillatory convergent irradiation as outlined above. Experience has shown that most of the cases occurring in practice can be covered by these three methods; moreover, these methods are precisely those for which the most complete therapeutic experience and dosage data are available.

The movement of the tube during irradiation is governed by a controller (*fig. 12*) mounted on a desk, placed behind a screen of lead glass outside the irradiation room. The three positions of the selector seen at the top of the controller correspond to the three methods of irradiation mentioned above. When stationary tube irradiation is selected, all the mechanisms for the various movements of the X-ray tube are locked, and the only remaining control is to switch on the radiation for the required period at the control desk. When the selector is turned to the position for rotational irradiation, the tube starts its movement automatically as soon as the H.T. is switched on at the control desk, and continues to travel to and fro between the two pre-adjusted end contacts until the expiry of the period set by the time switch of the apparatus. The tube then stops and the tube voltage is switched off. If several parallel bands are to be irradiated, the master switch seen in *fig. 12* below the method selector can now be used to shift the tube in the direction of traverse to the next irradiation band. Provided that the end contact for the traverse is pre-set to the required distance the tube may be allowed to proceed to the contact, its arrival there being indicated by a signal lamp; the rotational irradiation described in the above can then be repeated. On completion of this process, the master switch is turned to the other position and the tube then proceeds to the opposite pre-set end contact of the traverse; when the signal lamp indicates that

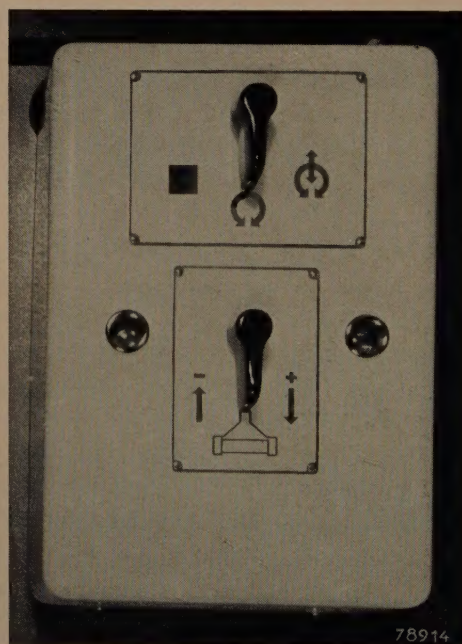


Fig. 12. Controller for automatic moving field irradiation. The selector for the three methods of irradiation is seen above, and the master switch for the traversing movement below.

this contact has been reached, the third band is irradiated⁸⁾. A locking mechanism is provided as a safeguard against accidental manipulation of the master switch during the rotational movement. To prevent accidental incorrect irradiation of the patient, this motion is governed by a centrifugal switch on the appropriate electric motor; no H.T. can be applied to the X-ray tube, and hence no radiation can be produced, unless the motor is running. Should one of the end contacts, or one of the associated change-over relays for the motor fail to operate, the entire apparatus is put out of action automatically by special safety end contacts so that the patient cannot be harmed, or the apparatus damaged by such failure.

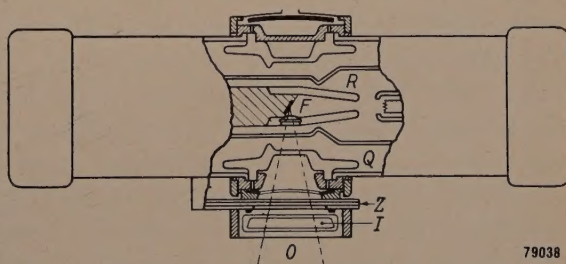
Finally, let us consider the third position of the selector, that is, oscillatory convergent irradiation. When this method is selected the speed of the traverse motor is reduced by a switch-over to 1/6 of the normal speed. As soon as the tube voltage is switched on, the tube starts its combined traversing and reciprocating movement. The time switch of the X-ray apparatus is set to the exact time required to cover the range of traverse between the particular positions of the end contacts; hence the radiation and the movement of the tube are switched off simultaneously as soon as the tube completes this movement. The traversing movement is also governed by a centrifugal switch on the motor and by safety end contacts in the manner described above for the rotational movement.

With the patient correctly positioned, the end contacts limiting the movement of the tube are adjusted, using a hand switch (*H* in fig. 5) to move the tube. Removing this hand switch from its hook automatically locks the tube voltage switch and thus safeguards the operator performing the adjustment against accidental exposure to X-radiation. The X-ray tube can be shifted at will in the directions of rotation and traverse by means of two levers on the hand switch. The tube positions corresponding to the limits of the desired movement can be located quite simply with the aid of the light-beam coincident with the direction of the X-rays, and the end contacts can then be set to these positions. In critical cases the entire pattern of the irradiation can be checked before it is administered, using the hand switch.

On completion of these preparations, the arms carrying the light-pointers are swung back to the

frame, the light source is removed from the beam aperture and a lead diaphragm is inserted in its place in the holder. Initially this diaphragm leaves an aperture corresponding to the size of the fluorescent screen used for the preliminary fluoroscopic check. Before irradiation is actually started, however, the diaphragm is pushed further into the holder so that it limits the cone of X-rays to the cross-section corresponding to the size of the lesion to be treated. If necessary a filter can be inserted in a holder in front of the diaphragm (as already mentioned, it is in principle unnecessary to use a heavy filter in moving field irradiation). The patient is then left alone in the irradiation room and the pattern of irradiation is regulated from the adjoining control room in the manner described.

We shall finally refer very briefly to a problem which is extremely important in this and every other method of deep therapy, viz. the determination of the lesion dose. In general, the lesion dose is measured with the aid of small ionization chambers, placed either in the immediate vicinity of the lesion during irradiation or in an equivalent position in a phantom previously exposed to a trial irradiation. In the case of rotational irradiation involving an almost completely circular movement of the X-ray tube it is possible to employ a simpler procedure, which consists in measuring simultaneously the dosage rate of the tube and the dose transmitted through the patient⁹⁾. The dosage rate of the tube is measured continuously by means of a large, flat ionization chamber, mounted between the filter holder and the diaphragm holder on the beam aperture in the shield (fig. 13), and connected to an



79038

Fig. 13. X-ray tube *R* and shield with built-in ionization chamber *I* for measuring the dosage rate of the tube. *F* focus, *O* beam aperture, *Z* filter mount, *Q* oil-bath for insulation and cooling.

indicating instrument on the control desk; the transmitted dose is determined by an integrating measurement with a sensitive ionization chamber mounted in the central ray of the X-ray beam behind the patient, on a movable mount attached

⁸⁾ The simple method of construction described here is of course possible only by reason of the fact that no more than three irradiation bands are employed, the middle band being irradiated first.

⁹⁾ W. Neumann and F. Wachsmann, *Strahlentherapie* **71**, 438-449, 1942.

to the fluorescent screen holder (see fig. 5). Although this method, as already noted, is applicable only to angles of rotation in the region of 360° , a new method has recently been developed whereby the dose absorbed by the lesion can be determined for other angles of rotation, however small, without the aid of phantom tests ¹⁰⁾.

Conclusion

In conclusion it may be worth mentioning once again the great scope in the choice of movement available to the user of the TU 1. This is primarily attributable to the fact that the apparatus is equipped with two separate, electrically controlled units, one for each of the two degrees of freedom of movement. This arrangement provides a method that is in a high degree automatic and largely foolproof against possible errors, without appreciable curtail-

ment of the therapeutic possibilities. In fact there is every reason to suppose from the experience gained so far, that this apparatus gives a general solution to the problems associated with normal X-ray deep therapy.

Summary. During X-irradiation of deep sited lesions in the body, the harmful effects of the rays upon adjacent organs and in particular upon the areas of skin exposed to the rays, can be obviated by moving the X-ray tube around the patient in a suitable manner during the process of irradiation. Owing to the relatively small size and weight of modern X-ray therapy units, this movement can now be made to take place automatically. The Müller TU 1 apparatus is designed for this purpose. Here the X-ray tube is capable of rotation about the horizontal patient, and can perform a traversing movement parallel to his longitudinal axis. Separate motors are used to actuate the two movements. Control of the motors is such that a very wide variety of motions can be accomplished automatically. In the TU 1 apparatus three automatically controlled methods of irradiation are provided, i.e. stationary tube, rotational and oscillatory convergent irradiation. This article includes a description of the equipment and a brief account of the provisions made to ensure correct positioning of the patient and to limit the movement of the tube to the desired range.

¹⁰⁾ H. Wichmann, Tabellen zur Dosierung bei Bewegungsbestrahlung, to be published shortly.

CHEATER CIRCUITS FOR THE TESTING OF THYRATRONS

I. MEASUREMENT OF GRID CURRENT

by M. W. BROOKER *) and D. G. WARE **).

621.387:621.385.38

The range of thyratrons now being produced commercially includes certain types which operate at high anode voltages and draw high currents. The conventional ways of thoroughly testing these valves under their full-load operating conditions would make excessive demands on the power supply. Attempts have therefore been made to devise "cheater circuits" which simulate full-load operation at only a fraction of the power load and cost of energy.

In Part I of their article the authors describe a cheater circuit which allows the measurement of grid current just before the valve strikes. The pre-striking grid current is an important check on valve quality. Part II will deal with another form of cheater circuit, designed for the life-testing of thyratrons.

In a high-vacuum triode with unsaturated emission the flow of anode current is limited mainly by a space charge of electrons. This in turn can be controlled at will by variation of the negative potential of the grid. In a gas-filled triode (thyatron) there is no such control and the grid acts only as a kind of trigger which determines when the valve shall fire. This, too, means a certain controllability, though of a slightly different nature from that in a vacuum tube. When the voltage applied to the grid is made less negative and ultimately reaches a certain critical level, anode current commences to flow; the positive ions produced neutralize the electronic space charge and the anode current rises rapidly to the value prescribed by the circuit parameters. This process is known as the firing or striking of the valve. Once a gas-filled valve has struck, the grid has no control over the current, as the effect of its potential is masked by a sheath of positive ions.

When a gas-filled valve is in the non-conducting state with the grid biased negatively, a grid current will flow. This is due to a number of effects, which will be explained later. The pre-striking grid current flows through the grid resistor and may disturb the accuracy of control of the valve. Indeed, if the grid current becomes relatively large and the grid resistance is high, it may be quite impossible to control the valve. It is therefore necessary to have an accurate method of measuring the pre-striking grid current, both as an aid in design and as a check on quality.

This article first reviews some known methods of measuring grid current in thyratrons and then

describes better methods, which are simple to use and which measure grid current under conditions identical with the full-load valve operating conditions.

Conventional methods of measuring grid current

The grid current is a thyatron before it strikes is actually the sum of several currents flowing in the same sense. It has components due to:

- 1) electrical leakage between the electrodes,
- 2) the flow to the grid of positive ions produced by electrons escaping control by the grid ("uncontrolled cathode emission"),
- 3) primary thermionic emission from the grid itself, and perhaps
- 4) photo-emission from the grid.

It is possible to measure some of these components individually. Thus the leakage current alone can be found by normal insulation measuring methods. The current due to uncontrolled cathode emission can be measured by putting a micrometer in the grid circuit and applying the rated anode voltage; the grid current-grid voltage may then be plotted. (The microammeter should be protected against overload, as the grid current rises to a high value when the valve strikes.) But the real problem is to measure it under actual operating conditions. It is in securing these conditions that the main difficulty lies.

The basic idea employed by most of the known methods of measuring the pre-striking grid current of gas-filled valves are given below.

The switch method

This method is very simple to set up and simple to use, but it only gives an approximate idea of the grid current under working conditions.

*) Mullard Radio Valve Co., Ltd., Mitcham, England.
 **) Formerly with Mullard Radio Valve Co. Ltd.

The procedure is to operate the valve with a resistive load at its rated mean anode current for a time sufficient to raise all the electrodes to their working temperatures. A switch is then operated which disconnects the load and connects anode to cathode and at the same time connects a negative voltage of, say, 100 V to the grid via a microammeter. The current read on this meter is called "the" grid current.

The advantages of this method can be listed as follows:

- 1) The method can be applied very easily to any type of thyatron.
- 2) The equipment is cheap.

The disadvantages are equally obvious, thus:

- 1) The current recorded decreases due to the valve electrodes cooling.
- 2) Leakage current (if present) is incorrectly measured owing to anode and grid voltages being abnormal.
- 3) Uncontrolled cathode emission is absent.
- 4) Ionization due to emission from other electrodes such as screens and anode is absent.

The cut-off method

A method generally used in the United States, known as the cut-off method, consists in operating the valve from an A.C. power supply, which may be the 220 volt mains, through a resistor which is adjusted to give the maximum rated mean anode current when the valve conducts for complete half cycles. After running like this for a long enough period for the valve to reach temperature equilibrium, the grid voltage is made more negative until the valve just fails to re-strike, and the voltage V_{g1} at the input side of the grid resistor is noted at the cut-off point. This is done with a low and a high grid resistance (R_{g1} , R_{g2}). If the critical grid current is represented by $I_{g\text{crit}}$, the critical voltage at the grid itself is given by $V_{g1} - I_{g\text{crit}}R_{g1} = V_{g2} - I_{g\text{crit}}R_{g2}$, V_{g1} and V_{g2} being the voltmeter readings. From this we find:

$$I_{g\text{crit}} = \frac{V_{g2} - V_{g1}}{R_{g2} - R_{g1}} \quad \dots \dots (1)$$

This method has a number of advantages over the previous one, viz.:

- 1) The grid voltage at the point at which the measurement is made is the normal critical grid voltage. Thus the electrical leakage current included in the measuring results is correct.
- 2) Any uncontrolled emission will be measured, but as this depends upon the applied anode voltage, it is necessary to perform the test at

the full rated anode voltage if any accurate result is to be obtained.

- 3) Grid emission is also measured at the proper voltage.

However, the method does not allow the full rated *peak* anode current to be drawn, as for a half-sine waveform, the peak-to-mean anode current ratio hardly exceeds 3, while modern thyratrons are rated for peak-to-mean ratios of 10 or even more. This disadvantage is important, because in general the valve voltage drop is higher when high peak currents are drawn; therefore the valve runs at a higher temperature, and the grid current is greater under such conditions.

Another disadvantage is that as the grid voltage is made more negative toward the cut-off point, the original half-sine waves diminish to quarter sine waves and the mean anode current correspondingly decreases to half its original value. Now in order to obtain an accurate reading of cut-off voltage, it is necessary to raise the negative grid voltage rather slowly, with the result that the valve cools appreciably during the time taken for the measurement. This of course means that the measured grid current is lower than the actual working grid current.

On the other hand, on switching from a low grid resistance to a high one, striking will occur earlier in the cycle, so the mean anode current will increase, making the valve hotter and this in turn increases the grid current. It was found that in some cases the grid current changed so rapidly that it was not possible to obtain any steady operating condition with a high grid resistance. This, of course, occurred with defective valves where the total grid current which flows is high, but for test purposes it is essential to be able to measure grid currents up to extremely high values.

The modified cut-off method with feedback

The drawbacks of the standard cut-off method have led to the design of a modified method. Here, the difficulties mentioned have been avoided by means of negative feedback. This method, which was the first to be developed by the authors, proved of considerable value in early thyatron development work by Mullard.

The basic method is shown in *fig. 1*. The anode voltage of the test valve is supplied from 220 V A.C. mains. The grid circuit includes a stabilized D.C. supply adjustable by a potentiometer supplying a positive voltage to the grid. A variable load resistor R_1 is in series with the cathode, and a group

of resistors R_g can be switched, one by one, into the grid circuit.

When an anode current flows, a rectified half-wave voltage appears across the load resistor R_1 . This voltage is smoothed by a filter $L_1-C_1-L_2-C_2$ and appears as a negative voltage at the grid of the valve

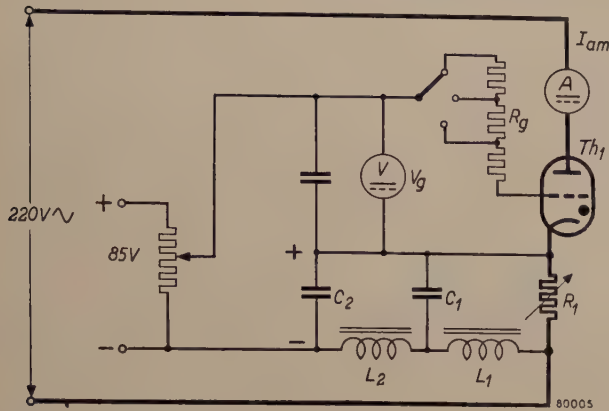


Fig. 1. Cut-off method for measuring the grid current of a thyatron (Th_1), with negative feedback. The D.C. voltage developed across the load resistor R_1 is smoothed by a filter $L_1-C_1-L_2-C_2$ and fed back with negative polarity to the grid of Th_1 , in opposition to an adjustable D.C. voltage from a stabilized supply (85 V). The resulting grid voltage V_g is read on a voltmeter, the mean anode current I_{am} on an ammeter. By means of a switch, various resistors R_g can be inserted into the grid circuit.

This negative voltage is partially counterbalanced by the stabilized supply, which acts in the opposite sense. Thus the striking of the valve is controlled by a (negative) grid voltage, which increases linearly with the mean anode current.

The self-compensating action of the circuit is best understood by reference to fig. 2. Consider the effect of a rise in grid voltage from level 1 to level 2 caused by a change in current flowing through the grid resistor. The valve will strike earlier in the cycle, the "firing angle" being reduced from α_1 to α_2 .

The mean anode current and the mean voltage across R_1 will therefore increase. A greater negative D.C. voltage is therefore fed back to the grid of the valve, thus tending to keep the anode current steady.

This self-compensating effect ensures stable running at a steady anode current, providing no attempt is made to fire the valve near the peak of the anode voltage curve. With firing angles greater than about 80° , instability and oscillation may set in because of the time delay in the filter circuit.

Using this new method, the variations of the mean anode current are reduced to a much lower level and it is easy to maintain a steady anode current, which is set by adjusting the load resistor.

The resultant grid voltage applied to the thyatron is read on the voltmeter V_g of fig. 1, and the grid currents may then be measured with a firing

angle of, say, 45° , as described above under the heading *The cut-off method*.

The chief advantage of the method just described is that measurements of grid current can be made without affecting the working conditions. However, it still suffers from the disadvantage that the peak anode current cannot exceed 5 times the mean anode current, owing to the firing angle being limited to about 80° ¹⁾. It is possible to overcome this disadvantage by superimposing on the D.C. bias an A.C. voltage (sinusoidal, or better still, pulse-shaped), leaving the rest of the circuit unaltered. By phase-shifting the A.C. voltage, firing angles up to 180° and smooth anode current control down to zero can then be obtained.

In the next section a method of measurement will be described which makes use of pulse firing to obtain stable operation at high peak-to-mean current ratios.

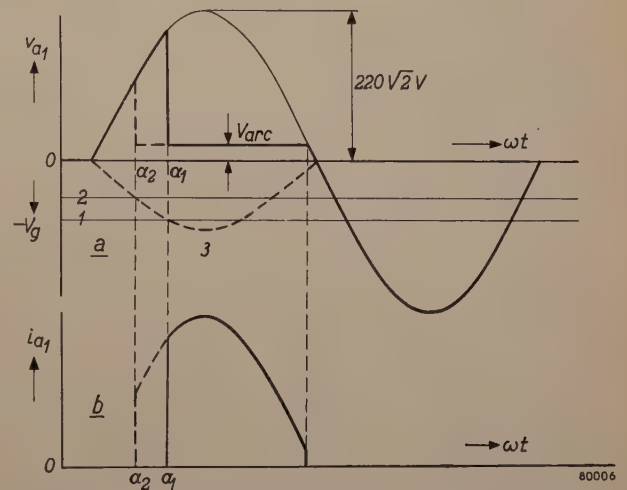


Fig. 2. Explanation of stabilizing effect of feedback in fig. 1. A rise in grid voltage V_g from level 1 to level 2 decreases the firing angle (determined by the point of intersection with the dotted critical grid voltage curve, 3) from α_1 to α_2 , thereby increasing the mean anode current I_{am} , i.e. diminishing V_g . This tends to keep I_{am} steady. V_{a1} voltage across Th_1 ; V_{arc} arc voltage; i_{a1} anode current; $\omega = 2\pi \times$ mains frequency; t time.

Cheater circuit

A disadvantage common to all methods mentioned above — so far as high-power thyratrons are concerned — is that the testing makes an excessive demand on the power supply, especially when voltages much higher than 220 V r.m.s. are to be used. Attempts have therefore been made to devise special circuits which simulate full-load operation at only a fraction of the power.

¹⁾ As can be shown by a simple calculation, the peak-to-mean anode current ratio for firing angles α up to 90° is given by $2\pi/(1+\cos \alpha)$, and for α between 90° and 180° by $2\pi \sin \alpha/(1+\cos \alpha)$, see fig. 3. The latter expression tends to infinity when α approaches 180° .

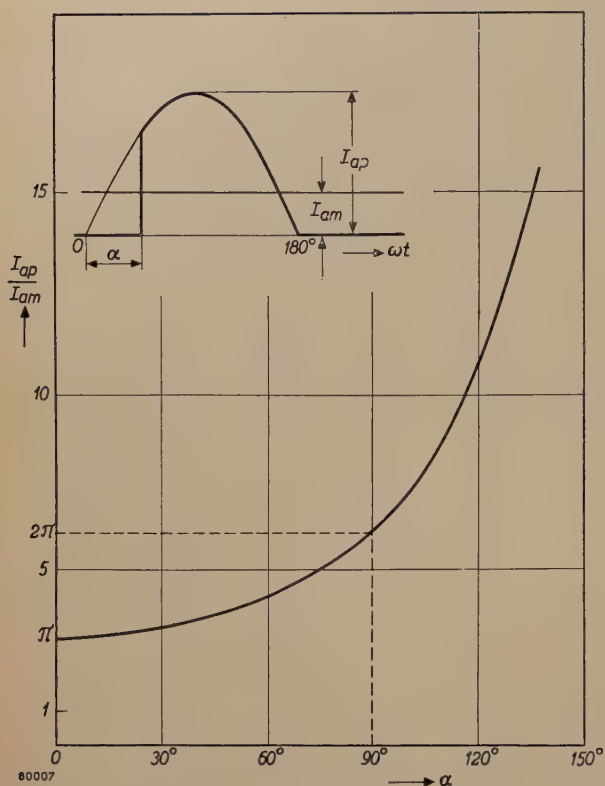


Fig. 3. Ratio of peak anode current I_{ap} to mean anode current I_{am} as a function of the firing angle α .

A characteristic fundamental to all thyatrons makes possible such circuits: the fact that once a valve has struck, the voltage across it drops to a low level, which is almost independent of the anode current. Although the peak anode voltage before striking may be, say, 1500 V, yet when carrying its full rated anode current the anode voltage V_{arc} is less than 20 V, just sufficient to maintain ionization (fig. 2). Providing that the voltage applied to a valve does not fall below this maintaining potential (arc voltage), the valve continues to conduct. If,

then, a circuit can be devised which switches automatically from a high to a low voltage supply immediately after the valve has struck, only a low surplus voltage will have to be taken up by the load, and the power economy will be considerable. Such a circuit is known — for obvious reasons — as a *cheater circuit*.

To provide a versatile circuit, useful in certain other tests, a special cheater circuit was devised. Its mode of operation is based on the same principles as the methods previously described for the cut-off method: the grid current is deduced from the change observed in the critical grid voltage at a given anode voltage when a resistor is switched into the grid circuit. Once again a D.C. bias is used for control and measurement, but the system of firing the valve is changed. A pulse triggering circuit is introduced, which ensures reliable firing at any point in the positive anode voltage half-cycle, and also plays an important part in the cheater action.

The main circuit of the new apparatus is shown in fig. 4. The valve under test Th_1 is connected to a 100 V A.C. supply, in series with a load resistor R_1 and an auxiliary thyatron Th_2 . It is connected also, via a large series resistor R_2 , to a high voltage A.C. supply. The high and low voltage supplies are connected so as to be in phase. In the grid circuit of Th_1 there is the usual bank of resistors R_g used in the actual measurement of grid current.

The cheater action of this circuit is best explained diagrammatically. Figs. 5a, b and c show the wave-forms of the voltages appearing across Th_1 and Th_2 and the current through Th_1 . Consider first Th_1 . In its non-conducting state, the voltage across it is the high one supplied by the high-tension transformer T_2 . If now the valve is caused by a pulse to strike at P, this voltage drops to about 10 V; because of R_2 , however, the current which flows through the test valve is small, say 10 mA. Considering now Th_2 , during the first part of the high-voltage cycle, the cathode of Th_2 is driven positive, which is, of course, equivalent to the negative voltage shown in fig. 5c. This negative voltage is much greater than the 100 V supply to the anode of Th_2 , which is therefore non-conductive. When Th_1 has struck, however, the large negative voltage on the anode of Th_2 disappears: it has then a positive anode voltage from the 100 V supply and it too can be fired by the same pulse through Th_1 and Th_2 . This current can be the full load current of the test valve Th_1 , which is thus being fired from a high-voltage supply (say 1500 V), but subsequently drawing its current from a low-voltage source (100 V).

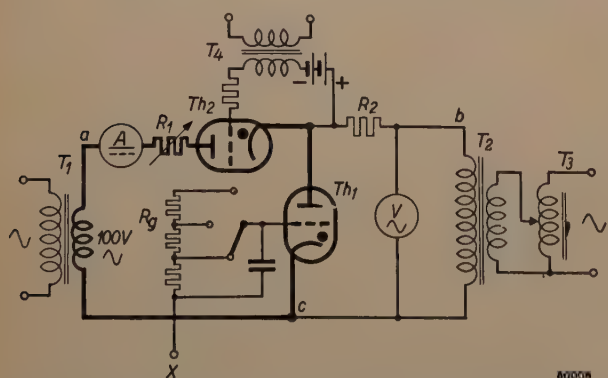
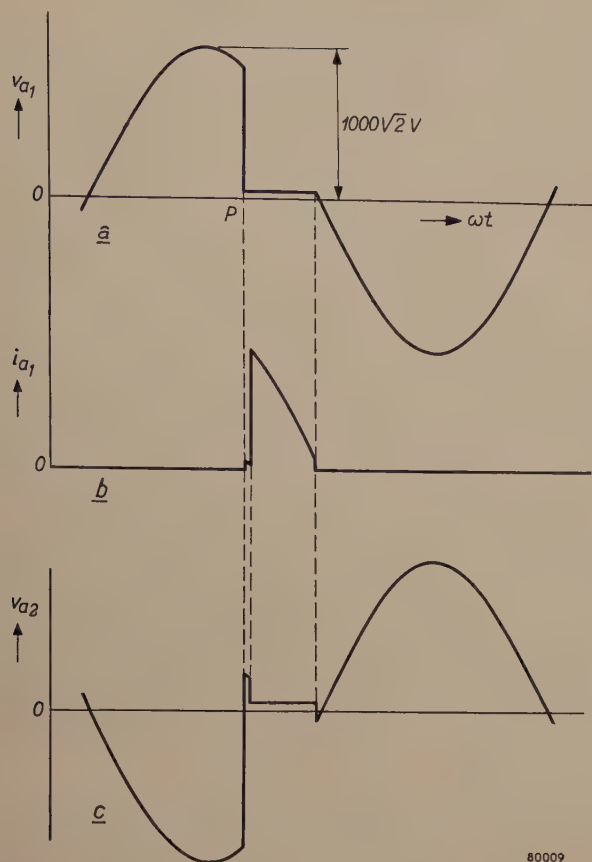


Fig. 4. Cheater circuit for measuring grid current under full operating conditions. Th_1 thyatron under test. Th_2 auxiliary thyatron. T_1 low voltage transformer (100 V). T_2 high voltage transformer, fed from variable autotransformer T_3 . R_1 load resistor. R_2 current limiting resistor in H.T. circuit. R_g bank of grid resistors. Firing pulses are applied at X and also to transformer T_4 (see fig. 6).



80009

Fig. 5. Explanation of cheater circuit of fig. 4.

- a) Voltage v_{a1} across valve under test, due to source of high tension (here supposed to be 1000 V r.m.s.).
 b) Current i_{a1} through test valve.
 c) Voltage v_{a2} across auxiliary valve.

Immediately before striking of test valve (at P), v_{a1} is high. Power consumption is low, owing to current being mainly drawn from low voltage source. (Firing of auxiliary valve is shown slightly later than striking of test valve.)

To provide a grid voltage for Th_1 , the circuit shown in fig. 6 is employed, which supplies both the D.C. component and the triggering pulse. The negative D.C. bias, which is variable up to -100 V, is drawn from a full-wave rectifier (not shown). The trigger pulse, which has an amplitude of 300 V and a duration of 50 microseconds, is generated as follows. An A.C. voltage of 50 V is applied to the control grid of a high-slope pentode Pe_1 . This A.C. voltage can be phase-shifted by means of a variable resistor R_3 . The valve is overloaded by such a voltage and therefore produces a square-wave anode current. This waveform is differentiated (C_4 - R_4) and the result applied to the grid of a Mullard 2D21 thyatron (Th_3), which forms a low-impedance output stage. The valve Th_3 is therefore caused to strike and so initiates the discharge of a capacitor C_5 via a choke L_5 and a resistor R_5 . The peak-shaped voltage which then appears across L_5 - R_5 is fed, via the capacitor C_6 , to the grid of the valve under test.

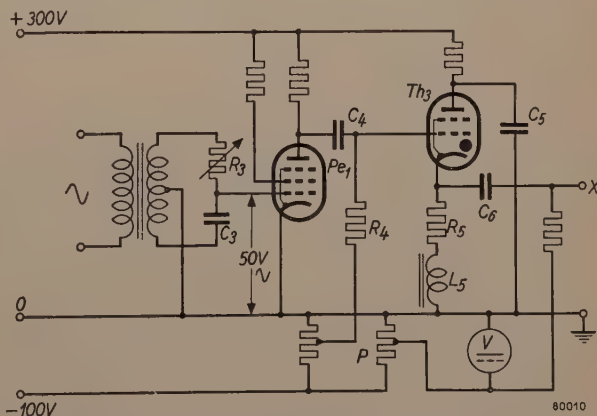
The grid of the auxiliary valve (Th_2 , fig. 4) is connected to a permanent D.C. bias in series with a transformer through which is fed the trigger pulse generated by the circuit of fig. 6.

Measurement of pre-striking grid current

Suppose a valve is set up in the above apparatus (fig. 4) and fired by the pulse at some time after

the occurrence of the peak anode voltage (firing angle $\alpha_1 > 90^\circ$). The pulse is also fed to the auxiliary valve Th_2 , so it too fires and allows full load current to flow through Th_1 and Th_2 in the way previously described. If now the negative grid bias of Th_1 is gradually reduced, the valve first continues to strike at the angle α_1 determined by the grid pulse, until the D.C. bias reaches a value equal to the critical grid voltage corresponding to the H.T. peak anode voltage. In the H.T. circuit the firing of Th_1 is then suddenly advanced from $\alpha_1 (> 90^\circ)$ to 90° . The grid voltage $V_{g,90}$ at which this happens can be read on a voltmeter. If the grid resistance is increased and the measurement repeated, a higher value of $-V_{g,90}$ will be noted. From the change in resistance and the change in $V_{g,90}$ the pre-striking grid current can be deduced with the help of equation (1), see above.

Fig. 7 represents the whole operation in terms of voltage and current wave-forms. It also helps to make clear exactly what is being measured and to bring out the distinction between this method and previous ones. Previously, the grid current measured was that at the moment when the valve struck; the valve was at its correct working temperature, but it was not subject to its rated peak anode voltage, and also it was impossible to fire the valve at angles greater than 90° . As pointed out earlier, the maximum peak-to-mean anode current ratio occurs when the valve is fired late in the positive anode voltage half-cycle. It was therefore impossible, using previous methods, to test a valve with both maximum anode voltage and maximum peak



80010

Fig. 6. Circuit providing firing pulses and D.C. bias for cheater circuit (fig. 4). A transformer connected to R_3 - C_3 supplies 50 V A.C., with variable phase shift, to control grid of pentode Pe_1 (EF 91). Square-wave anode current of Pe_1 is differentiated by C_4 - R_4 , producing pulses which fire output stage thyatron Th_3 (Mullard 2 D 21). Th_3 being fired, capacitor C_5 discharges through Th_3 , R_5 and L_5 (choke L_5 helping to extinguish Th_3). Via coupling capacitor C_6 , voltage pulse across R_5 - L_5 is applied to grids of test valve (at X) and of auxiliary valve (via transformer T_4 , see fig. 3). Variable D.C. bias is obtained from potentiometer P .

and mean anode currents, and these are the very conditions which lead to maximum grid emission, leakage and uncontrolled cathode emission — i.e. to maximum grid current.

The new method has no such drawbacks. The grid current is necessarily measured when the anode voltage is at its peak value, whatever the peak-to-mean anode current ratio. The value obtained, is therefore a true indication of the worst possible grid current likely to flow under any given conditions.

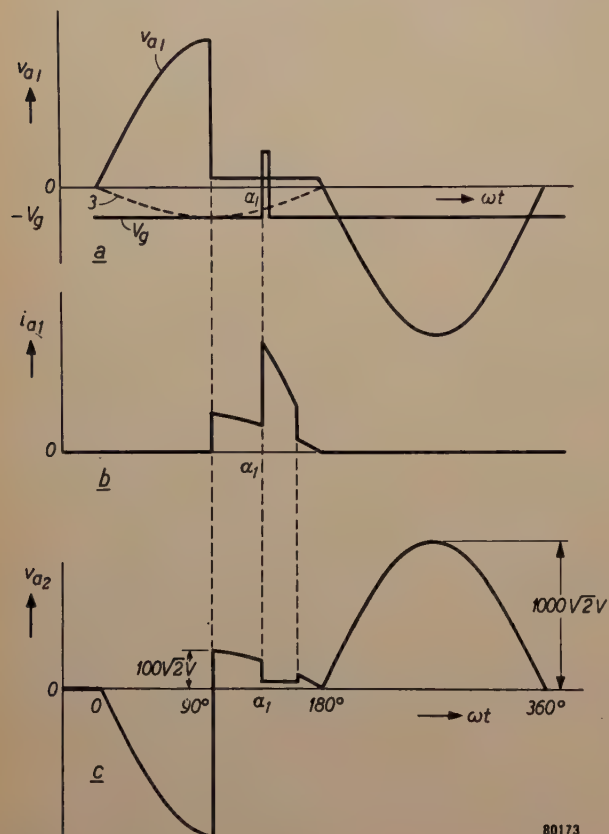


Fig. 7. Explanation of pre-striking grid current measurement with cheater circuit of fig. 4.

At (a), D.C. bias of test valve Th_1 is shown adjusted to top of critical grid voltage (curve 3), causing Th_1 to fire at peak of H.T. anode voltage (see b). Auxiliary valve Th_2 is fired by a pulse (firing angle $\alpha_1 > 90^\circ$), initiating main current through both valves. Voltage v_{a2} across Th_2 is shown at (c).

It will be appreciated that the time available for de-ionization of the auxiliary valve Th_2 is very short. In fact, if t_1 denotes the instant where Th_2 extinguishes (i.e., where the anode voltage of both valves in series has dropped to, say, 30 V), and t_2 the instant where v_{a2} , in the subsequent

half-cycle, reaches the value of, say, 20 V at which ionization becomes possible again, and if the applied A.C. voltages are 100 V and 1000 V r.m.s., then

$$100 \sqrt{2} \sin \omega t_1 = 30$$

$$\text{and } (1000-100) \sqrt{2} \sin \omega t_2 = 20$$

(with $\omega = 2\pi \times 50$ radians per second, and the load resistors supposed to be non-inductive). If τ is the interval between t_1 , and the moment where the A.C. voltages pass through zero, and τ_2 the interval between this moment and t_2 , then we find from the above equations: $\tau_1 = 680 \mu\text{sec}$ and $\tau_2 = 50 \mu\text{sec}$. If the high voltage is increased to 10 kV, this merely reduces τ_2 to 4 μsec , leaving τ_1 unaffected. Thus it is clearly possible to use this circuit at very high voltages, provided the low voltage does not exceed 100 V r.m.s. and provided the valve de-ionization time does not exceed 500 μsec . A circuit of this type has been successfully used for testing mercury thyratrons at voltages up to 30 kV peak.

Summing up, this method of measuring grid currents has the following advantages:

- 1) It measures the maximum grid current flowing under any given conditions of loading for any anode voltage up to, say, 30 kV peak.
- 2) It economizes in power when testing thyratrons drawing high currents at high voltages.

The power required to operate this circuit for a 6 A thyatron at 100 V, including auxiliaries, amounts to 800 W only. Comparing this with the power required for a straight test at, say, 1000 V, it is evident that the advantages of this circuit are very real, and when voltages of 20 kV or more are required, it is clear that a direct test method is prohibitive, so that this circuit is not merely useful but a necessity.

Summary. Part I of this article deals with the measurement of the pre-striking grid current of thyratrons under full operating conditions. Several conventional circuits are reviewed, and shown to be not entirely satisfactory. One of the drawbacks when large thyratrons are to be tested, is the high power consumption. A "cheater circuit" has therefore been devised, which simulates the desired working conditions with a great economy of power. Here the valve is part of a low-current H.T. circuit, until immediately after firing, when it is automatically changed over to a L.T. circuit, in which the full rated anode current is permitted to flow. This system allows the measurement of the pre-striking grid current under any conditions of loading.

CONDITIONS FOR SQUARE HYSTERESIS LOOPS IN FERRITES

by H. P. J. WIJN, E. W. GORTER, C. J. ESVELDT and P. GELDERMANS.

538.23:621.313.134

Since ferrites were introduced commercially by Philips nearly ten years ago, the applications of these soft magnetic materials have enormously increased. The further development of these materials has been influenced by the fact that it has been found possible to manufacture them with properties specially adapted to particular purposes. The present article deals with the fundamental conditions for obtaining ferrites with rectangular hysteresis loops.

Introduction

Magnetic cores with approximately rectangular hysteresis loops have a wide range of application. They are used for example in the so-called "magnetic memory"¹⁾ of computing machines and automatic pilots, and for magnetic switching elements.

For a memory element, the requirements are that when a square pulse of a certain height is passed through the magnetizing coil, the core shall revert to its original condition after passage of the pulse but when a pulse of *double* this height is passed through the coil, the magnetization of the core shall be *reversed* after passage of the pulse. When the material is used for switching elements, the magnetization must not be affected by a positive pulse, but must be reversed by a negative pulse of the same height.

The pulses employed in these techniques are usually of very short duration, so that, during the pulse, the variation in the current, di/dt , assumes very high values, as a result of which rapid variations dB/dt occur in the induction, and eddy currents are produced.

It is important that the magnitude of these eddy currents should be minimized. In ferromagnetic metals (nickel-iron alloys such as "Hypenik" and "Deltamax"²⁾) this is to a limited extent achieved by building up the core from very thin insulated laminations of the material; in practice, however, it is difficult to construct such laminated cores to give nearly rectangular hysteresis loops.

Magnetically soft materials such as ferrites³⁾,

¹⁾ J. A. Rajchman, RCA rev., **13**, 183-201, 1953. A. Wang, J. appl. Phys. **21**, 49-54, 1950. Some specific instances are reviewed in F. van Tongerloo, T. Nederlands Radiogenootschap **18**, 265-285, 1953, No. 11.

²⁾ See for example R. M. Bozorth, Ferromagnetism, Van Nostrand, New York, 1952.

³⁾ J. L. Snoek, Philips tech. Rev. **8**, 353, 1946; J. J. Went and E. W. Gorter, The magnetic and electrical properties of Ferroxcube materials, Philips tech. Rev. **13**, 181-193, 1951/1952, referred to hereafter as I. As in I, the present article uses the rationalized Giorgi (M.K.S.) system, in which B is measured in Wb/m^2 and H in A/m ($\mu_0 H$ in Wb/m^2). $B = 10^{-4} \text{ Wb/m}^2$ corresponds to $B = 1$ gauss, and $\mu_0 H = 10^{-4} \text{ Wb/m}^2$ ($H = 79.5 \text{ A/m}$) to $H = 1$ oersted. The formula $\mu_0 = 4\pi \times 10^{-7}$ volt seconds/ampere metres. The formula $B = \mu_0 H + J$ takes the place of $B = H + 4\pi I$ in the electromagnetic c.g.s. system. If $J = 1 \text{ Wb/m}^2$, $4\pi I = 10,000$ gauss and $I \approx 800$ gauss.

which are at the same time poor conductors, offer considerable advantages over the use of laminated ferromagnetic metals in pulse applications (given that these materials can be made with rectangular hysteresis loops⁴⁾).

Definitions of certain quantities

One or two concepts will now be introduced which are essential to a consideration of the problem⁵⁾.

The loop depicted in fig. 1 (full line) is the hysteresis loop of a ferrite. It represents the magnetization J plotted against the magnetic field H for values

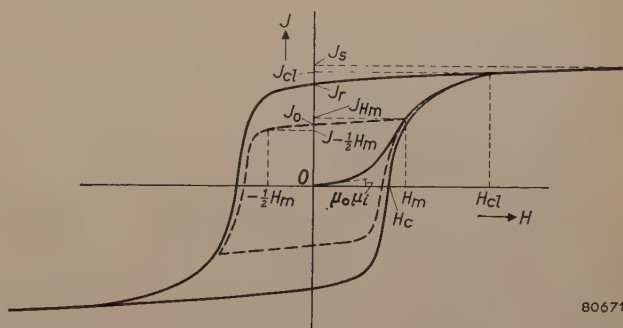


Fig. 1. Hysteresis loop of a ferrite.

of H which decrease from large positive to large negative values, and then revert to the positive value. The value of the field at which the magnetization is zero is known as the coercive force H_c of the material⁶⁾. On decreasing the field from a large value, the point at which the magnetization

⁴⁾ E. Albers-Schoenberg and D. R. Brown, Electronics **26**, April 1953, p. 146.

⁵⁾ For a more detailed discussion of these concepts and their physical basis see J. J. Went, Philips tech. Rev. **10**, 246-254, 1948/1949.

⁶⁾ In magnetic materials a distinction is made between a coercive force for the induction, BH_c , i.e. the field strength at which the induction B is zero, and a coercive force for the magnetization, JH_c , the field strength at which the magnetization J is zero. In general, BH_c and JH_c differ because $B = \mu_0 H + J$, and B and J do not become zero at the same time. In the materials discussed here the values of H are so small that the difference may be disregarded and the single symbol (H_c) employed.

begins to diverge from its previous values is denoted H_{cl} ; the corresponding magnetization is denoted J_{cl} . For fields $H > H_{cl}$ the variations in the magnetization are reversible. Smaller hysteresis loops are also obtainable, as shown for example by the dotted line in fig. 1, with extreme field values of $+H_m$ and $-H_m$ ($H_m < H_{cl}$). As a measure of the effectiveness of ferrites for the cores of memory devices the concept of "squareness" is introduced, defined as:

$$R_s = \frac{B_{-\frac{1}{2}H_m}}{BH_m}$$

or, what is practically equivalent,

$$R_s = \frac{J_{-\frac{1}{2}H_m}}{J_{H_m}} \dots \dots \dots (1)$$

The demoninator and numerator of the latter represent respectively the magnetization for a field $+H_m$ and that for a field $-\frac{1}{2}H_m$. It will be clear that R_s is also a function of the maximum field H_m determining the size of the loop. When R_s is measured as a function of H_m it is found that a maximum occurs for a certain value of H_m ; let this maximum be denoted by $(R_s)_{\max}$. With ferrites for which $(R_s)_{\max} > 0.7$, this value of H_m is roughly equal to H_c .

When ferrites are employed as switching elements the ratio J_0/J_{H_m} is important; J_{H_m} represents the above mentioned magnetization for a field H_m , and J_0 the remanent magnetization after removal of the field (see fig. 1). J_0/J_{H_m} is a function of H_m , and the maximum, $(J_0/J_{H_m})_{\max}$, of this ratio is also of interest.

General considerations

Magnitude of the remanent magnetization

Consider as the starting point the demagnetized condition, that is, point O in fig. 1. It may be taken as generally known that in this condition the material is divided up into "Weiss domains" within which the material is uniformly magnetized (see ⁵⁾). The magnetization vector in each of these Weiss domains lies in a certain direction (the preferential direction) and the magnetization averaged over all the domains is zero. The preferential direction of magnetization in each domain is determined by three factors, namely the crystal anisotropy, the stress anisotropy and the shape anisotropy. These factors will be discussed presently. Very small external magnetic fields turn the magnetization vectors away from their preferential orientation, towards the direction of the applied field. The extent

to which this is possible in the case of sintered ferrites is represented approximately by the quantity μ_i , the initial permeability ⁷⁾ (see fig. 1).

When the material is magnetized by a very strong field, all the magnetization vectors are parallel to each other and there is no longer any division into Weiss domains. This corresponds to the saturated state with magnetization J_s (see fig. 1). If the field be now gradually reduced to zero, the magnetization vectors turn from the direction of the field towards the nearest preferential directions as determined by the anisotropies mentioned above.

When the field H is zero a magnetization J_r remains (the remanence). For an ideal rectangular loop $J_r/J_s = 1$. If H be varied slightly, starting from the remanent state, a permeability μ_{rem} will be found which is again determined by the rotation of the magnetization vectors. The magnitude of the ratios J_r/J_s and μ_{rem}/μ_i , corresponding to the three kinds of anisotropy, will now be evaluated. The significance of the second of these ratios will appear later.

a) Crystal anisotropy. In nearly all cubic ferrites it has so far been found that the body diagonal is the preferential direction of the magnetization; there are accordingly eight such preferential directions. The magnetization energy per unit volume of a material whose magnetization vector is defined by the direction-cosines (with respect to the cubic axes) α_1 , α_2 and α_3 , is given to a first approximation by:

$$E = K(\alpha_1^2\alpha_2^2 + \alpha_1^2\alpha_3^2 + \alpha_2^2\alpha_3^2) \dots \dots (2)$$

In this expression, K may be both positive and negative. In materials with positive K , the value of E is at a minimum when one α is equal to unity and the others are zero, that is, when the magnetization vector is parallel to one of the sides of the cube.

In most ferrites, however, and also in some metals such as nickel, K is negative. E is then at a minimum when the factor between brackets in (2) is at a maximum, viz. when $\alpha_1 = \alpha_2 = \alpha_3$. The magnetization vector is then parallel to one of the body diagonals of the cube. If the crystal anisotropy is the only anisotropy present, when the field is reduced to zero after saturation in a strong field, the magnetization vectors of the Weiss domains in polycrystalline materials turn back from the direction of the field to the nearest cube diagonal (a (111)-direction).

⁷⁾ In contrast with article I, μ_i is taken as the relative permeability. The corresponding absolute permeability is $\mu_0\mu_i$, for which the symbol μ_i was used in I. The same applies to the quantity μ_{rem} introduced later.

Since there are eight preferential directions, the vectors revert to directions which are all contained within the solid angle $\pi/2$ (fig. 2). According to calculations by Gans⁸⁾, this leads to $J_r/J_s = 0.87$ and $\mu_{rem}/\mu_i = 0.36$.



Fig. 2. a) Distribution of the magnetization vectors in the Weiss domains in demagnetized polycrystalline materials. b) As above for the remanent state when (negative) crystal anisotropy predominates.

b) *Stress anisotropy.* It is well-known that the length of a rod of magnetic material changes with its magnetization; this property is known as magnetostriction. A distinction is made between positive and negative magnetostriction according to whether the magnetization is accompanied by an expansion or a contraction in the direction of magnetization.

If strains are present in the material as a result of elastic deformation, the magnetization tends to be so oriented that the accompanying variations in length oppose these strains. If the stress anisotropy predominates there will be only two preferential directions for the magnetization at every point in the material. In the case of negative magnetostriction (as usually found in ferrites), these directions correspond at each point to the two orientations at which the magnetization vectors are parallel to the greatest compressive strain or the smallest tensile strain. Here, too, the magnetization vectors turn back to the nearest preferential direction when the field is reduced to zero from the saturation value. For a random distribution of the strains in the material the vectors revert to preferential directions distributed over a solid angle of 2π (see fig. 3b). Under these conditions it has been calculated that $J_r/J_s = 0.5$.



Fig. 3. a) As fig. 2a.

b) Distribution of the magnetization vectors for the remanent state when stress anisotropy predominates.

⁸⁾ R. Gans, Ann. Physik 15, 28, 1932.

For ferrites with small crystal anisotropy but with a large magnetostriction coefficient, it is possible, when sufficiently large external forces are applied, that the latter determine the preferential direction of the magnetization. This has been demonstrated in the Eindhoven Laboratory by G. W. Rathenau and G. W. van Oosterhout in the following manner. A ring of glass was melted onto the outer cylindrical surface of a ring of Ferroxcube⁹⁾. The coefficient of expansion of the glass was slightly higher than that of the Ferroxcube, so that after cooling to room temperature the Ferroxcube was subjected to tangential compression. The magnetization caused by the negative magnetostriction was therefore parallel to the predominant strain. Consequently the strains in the ferrite were no longer distributed in a random manner, but mainly in one direction only, so that at every point in the material only two orientations of the magnetization were possible, viz. parallel and antiparallel to the strain. The remanence after removal of a field parallel to the compression (i.e. a tangential field) can thus theoretically assume a value equal to the saturation magnetization $J_r/J_s = 1$. Fig. 4 shows a family of hysteresis loops plotted

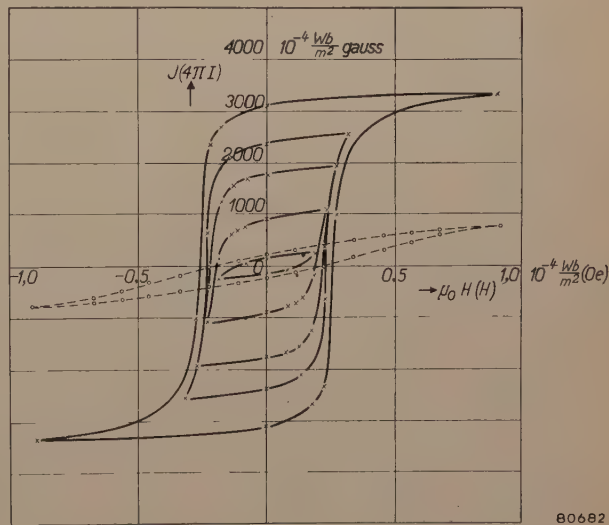


Fig. 4. Family of hysteresis loops for a ring of Ferroxcube IVA enclosed by a band of special glass. Dashed curve: hysteresis loop for Ferroxcube IVA without glass (see text).

from measurements on a ring of Ferroxcube IVA enclosed in glass. The loop drawn in broken lines is that of the ring without the glass. A great advantage of this type of material, with its rectangular hysteresis loop, is the low coercive force.

⁹⁾ Netherlands Patent application No. 175120, dated Jan. 1953.

Similar results have been obtained by enclosing a ferrite ring in synthetic resin ¹⁰).

If a polycrystalline material, prepared in the demagnetized state (O, fig. 1) by cooling from a temperature above the Curie point, contains no strain the direction of the magnetization vector in each Weiss domain is determined by the crystal anisotropy (disregarding shape anisotropy, see c). The magnetization vectors of the Weiss domains are then oriented in the above-mentioned preferential directions. When the material is magnetized and then brought into the remanent state, a large number of the individual magnetization vectors are turned from their original preferential direction into another. In general, this will be accompanied by a change of shape of individual crystals. For example, if the body diagonals are the preferential directions in cubic ferrites, the length of the body diagonal will depend on whether the magnetization vector is parallel to this diagonal or not. The corresponding difference in length is called the "magnetostriction in the preferential direction", λ_{111} . Even if there is no strain present in a polycrystalline material in the demagnetized state, there may nevertheless be strains present in the remanent state, unless $\lambda_{111} = 0$. In this particular case, the magnitude of the remanence is determined by the crystal anisotropy only: this is a requirement for high remanence ¹¹).

The results of measurements on a series of mixed crystals of nickel ferrite and ferrous ferrite shows the importance of magnetostriction in the pre-

ferential direction. Fig. 5 shows the magnetostriction λ plotted against the magnetic field H for polycrystalline preparations of mixed crystals of Fe_3O_4 and NiFe_2O_4 . The saturation magnetostriction (the value of λ for effective saturation) of these materials is $+41.6 \times 10^{-6}$ and -22×10^{-6} respectively, so that it may be expected to

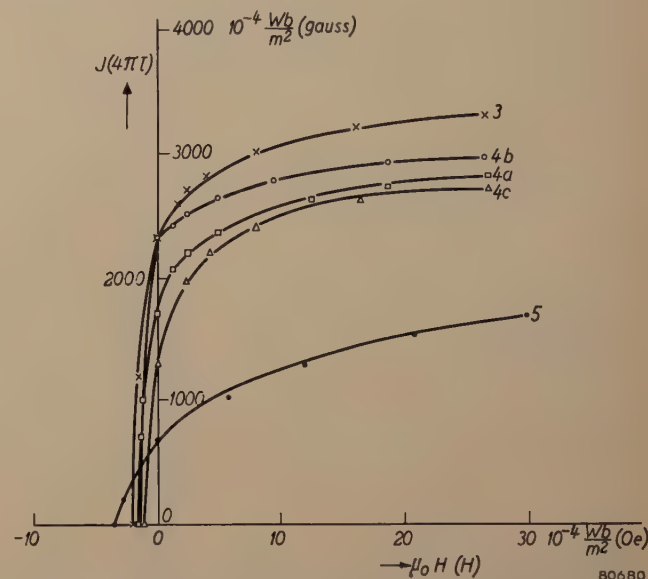


Fig. 6. Upper branch of the hysteresis loop for decreasing fields, for some of the ferrites in fig. 5.

be zero for a mixed crystal with a certain ratio of these constituents. It is, in fact, seen from fig. 5 that the saturation magnetostriction λ_s of $\text{Ni}_{0.56}\text{Fe}_{0.44}^{2+}\text{Fe}_2^{3+}\text{O}_4$ is very small ($\lambda_s = -0.8 \times 10^{-6}$). It was shown earlier, however, that it is the magnetostriction in the *preferred direction* that must be small in order to obtain a rectangular hysteresis loop. It can be shown quite simply that the sign of the magnetostriction of a specimen in a field of the same order of magnitude as the coercive force (i.e. $\mu_0 H_c \approx 10^{-4} \text{ Wb/m}^2$, $H_c \approx 1$ oersted, for mixed nickel-ferrous-ferrites) is the same as the sign of the magnetostriction in the preferred crystallographic direction. Fig. 5 shows that the sign of the preferential magnetostriction is reversed in compositions occurring between those of samples 4a and 4b ($\text{Ni}_{0.7}\text{Fe}_{0.3}^{2+}\text{Fe}_2^{3+}\text{O}_4$ fired at 1350°C in a current of gas consisting of 600 ml carbon dioxide and x ml nitrogen with 10% hydrogen, per minute ¹²)).

Part of the hysteresis loops of a number of the ferrites referred to in fig. 5 are shown in fig. 6. It

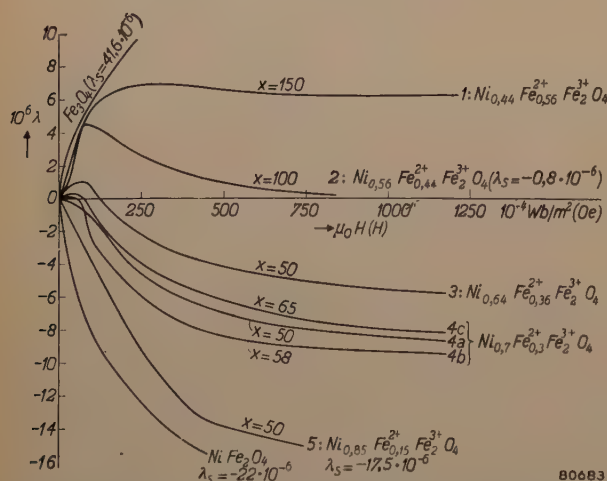


Fig. 5. Magnetostriction as a function of the magnetic field in polycrystalline samples of mixed crystals of nickel ferrite-ferrous ferrite. All samples were fired at 1350°C , but in gas currents of different composition, viz. 600 ml/min $\text{CO}_2 + x$ ml/min of a mixture of 90% N_2 and 10% H_2 . The value of x and the chemical composition of the ferrites are shown in respect of each curve.

¹⁰) H. J. Williams, R. C. Sherwood, Matilda Goertz and F. J. Schnetler, Commun. Electr. 9, 531, 1953.

¹¹) For these considerations we are indebted to J. Smit of the Eindhoven Laboratory.

¹²) The difference in the reducing power of these gases results in a slight displacement in the ratio of Ni^{2+} to Fe^{2+} in the ferrite. The quantity of NiO or FeO that may occur as second phase can be disregarded, in comparison with the volume of the pores.

can be seen that samples 4a and 4b do actually yield the anticipated greater squareness compared with the other materials.

c. Shape anisotropy. It is well known that when an open magnetic circuit is magnetized an opposing field is produced, i.e. partial demagnetization occurs, due to the "free poles" at the extremities. This opposing field, which may be regarded as due to shape anisotropy, is proportional to the magnetization. Although this article is concerned only with magnetic circuits which can be considered macroscopically as closed, we are nevertheless to a large extent concerned with demagnetization due to shape anisotropy in view of the more or less porous structure of the ferrite (see fig. 10). The porosity of the sintered material varies between 1% and about 25%, and the effect of the air inclusions is such that the field H_{int} in the material is weaker than the applied field H_{ext} . In general it can be said that this difference is proportional to the magnetization of the material:

$$\mu_0(H_{\text{ext}} - H_{\text{int}}) = NJ \quad \dots (3)$$

where N is a constant depending on the porosity.

In consequence of this, the measured hysteresis loop differs from that which would be obtained if the material were free from cavities or pores (see fig. 7). This effect can be regarded as a "shearing" of the

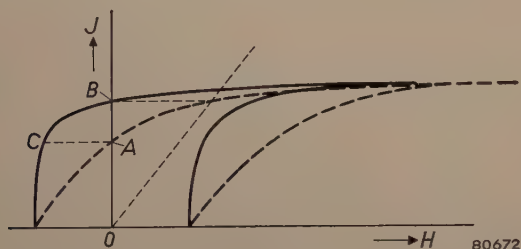


Fig. 7. Effect of "shearing" in the apparent shape of the hysteresis loop.

hysteresis loop. It will be seen from the figure that, owing to the shearing, the ratio J_r/J_s is considerably reduced, since J_r decreases whilst J_s of course remains constant. It may be noted that in the absence of shearing, the state corresponding to the point B is typified by a distribution of the magnetization vectors as in fig. 2b or 3b, according to which kind of anisotropy predominates. When shearing occurs, the point A is only apparently the remanent state; in fact the material is in a demagnetizing field $\mu_0 H = -NJ$, so that the actual state of the material is as shown at C. The distribution of the vectors is now very different from that in figs. 2b and 3b, and more resembles that of the demagnetized

condition (figs. 2a and 3a). It is also to be expected that μ_{rem}/μ_i will now be more nearly equal to unity, even in the case of predominant crystal anisotropy. In ferrites with equal saturation magnetization J_s and with similar porosity (i.e. equal N), the smaller the coercive force of the ferrite, the greater the influence of the demagnetizing field on the hysteresis loop.

Of possibly greater importance than the "shearing" is the effect of the porosity on the preferential direction of the magnetization at every point in the material. It is to be expected that in porous materials the direction of magnetization at each point will be largely determined by the direction of the demagnetizing field at the point. These demagnetizing fields result in only one preferred direction at each point, so that a low value of J_r/J_s may be anticipated.

To obtain "rectangular" hysteresis loops, the ratio J_r/J_s should be as nearly as possible equal to unity. With polycrystalline materials this can best be approximated when the crystal anisotropy predominates over the other anisotropies. It is especially important to ensure that shape anisotropy is absent: this means that porosity must be as low as possible. It is then found that $J_r/J_s = 0.87$. Higher values could be obtained if it were possible to ensure that the crystals are so oriented that all their body diagonals are parallel; this could even yield $J_r/J_s = 1$. This possibility cannot be pursued further here.

The coercive force

From the point of view of the application of ferrites with rectangular hysteresis loops it is important that the coercive force H_c shall be as small as possible. This is because H_c determines the number of ampere-turns necessary to reverse the direction of the remanent magnetization in the core. The coercive force is related to the field strength needed to displace the boundaries between the Weiss domains i.e. the Bloch walls. These "walls" are fixed at certain locations in the material as a result of internal strains and non-magnetic inclusions. It is to be expected that such walls in ferrites will be fixed to air pores which usually occur in a far greater number than in metals. We may therefore, for a moment, consider Néel's theory¹³), which gives an insight into the effect of porosity on the magnitude of H_c . Néel points out the fact that the internal stray magnetic fields caused by inclusions in ferromagnetic materials

¹³) L. Néel, Ann. Univ. Grenoble, **22**, 299-343, 1946, and Physica **15**, 225-234, 1949.

are limited to smaller domains when the Bloch walls pass *through* the inclusions. This is illustrated in *figs. 8a* and *b*. The magnetic “charges” of opposite sign are closer to each other in *b* than in *a*, which

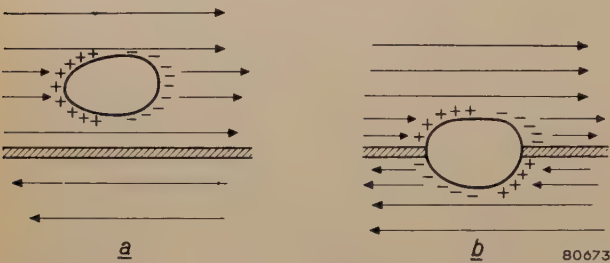


Fig. 8. Effect of inclusions or pores on the energy in a Bloch wall (Néel ¹³)
a) wall not intersecting the cavity.
b) wall intersecting the cavity.

means that the total magnetic energy is considerably less in *b* than in *a*. The location of the Bloch walls at which minimum free energy occurs is

where *p* represents the porosity of the material ¹⁴). The relationship between *p* and *H_c* in the range of Ni-Zn ferrites of differing properties has been investigated experimentally (see *Table I*), and the value of *H_c*, as computed from formula (4), is shown in the last but one column, *|K|* being calculated from μ_i on the assumption that μ_i is determined only by rotation (i.e. $\mu_i - 1 = \frac{1}{2} J_s^2 / \mu_0 |K|$). It is seen that in the range of porosities considered, *H_c* does depend on the porosity. If a low value of *H_c* is to be attained, the ferrite must be well sintered during preparation to obtain as low a porosity as possible. This can be achieved by firing at a high temperature, by employing a ferrite having a relatively low melting point, or by adopting a suitable ceramic technique. In the last two instances a high temperature is avoided, thus minimizing chemical reduction of the ferrite with its adverse consequences on the magnetic and electrical properties.

Table I. Relation between porosity and coercive force of nickel-zinc ferrites.

Ferro-cube IV Type	Firing temp. °C	Chemical composition in mole % (remainder FeO + Fe ₂ O ₃)		Porosity <i>p</i> %	Saturation magnetization		Initial permeability μ_i	Coercive force $\mu_0 H_c : 10^{-4}$ Wb/m ² <i>H_c</i> : oersted	
		NiO	ZnO		J_s 10 ⁻⁴ Wb/m ²	<i>I_s</i> gauss		per Eq. (4)	measured
A	1250	17.5	33.2	8.9	3650	292	650	0.4	0.4
B	1250	24.9	24.9	15.4	4150	332	230	2.0	1.4
C	1250	31.7	16.5	22.5	4012	321	90	6.2	4.0
D	1250	39.0	9.4	24.3	3537	283	45	10.4	6.8
E	1250	48.2	0.7	24.8	2450	196	17	16.1	13.7
A	1450	17.5	33.2	9.5	3620	290	470	0.6	0.3
B	1450	24.9	24.9	3.2	4750	380	312	0.4	0.4
C	1450	31.7	16.5	8.0	4760	381	86	2.7	1.1
D	1450	39.0	9.4	8.9	4260	341	63	3.5	1.7
E	1450	48.2	0.7	9.9	1688	135	42	3.7	3.2

therefore that at which the wall intersects as many air pores as possible. The coercive force is then the field strength necessary to dissociate a wall from its air pores, and this coercive force will be related to the concentration, as well as to the size, of the air pores. It has been found that inclusions or pores of diameters comparable to the Bloch wall thickness exercise the greatest influence on *H_c*. According to Néel’s theory, the coercive force *H_c* in the case of negative crystal energy (*K* negative), when the absolute value of *K* is high compared with J_s^2 / μ_0 (which applies to the ferrites considered here), is given by the formula:

$$H_c = \frac{4|K|p}{3\pi J_s} \left[0.39 + \frac{1}{2} \ln \frac{3J_s^2}{4\mu_0 |K|} \right], \quad . . \quad (4)$$

High remanence and small coercive force
Let us now briefly summarise the conditions to be fulfilled in order to obtain materials with square hysteresis loops (i.e. with a high remanence, which implies a high value of J_r / J_s), and suitable for practical purposes (i.e. having a small coercive force).
1) We have seen that if J_r / J_s is to be high, the crystal anisotropy must be predominant. A high value of $|K|$ implies a low value of μ_i , if μ_i originates only from rotational processes. The aim, then, is to produce a ferrite of fairly low initial permeability.

¹⁴) Thus (1-*p*) is the ratio of the macroscopic (or apparent) density of the material to the microscopic (or true) density. The latter can be determined by X-ray diffraction methods, the former by the ordinary methods of density measurement.

At the same time it follows from formula (4) that the coercive force H_c increases with $|K|$, so that the crystal energy must not be so great that H_c assumes undesirably high values.

2) The porosity should be as small as possible; demagnetizing fields are then small and H_c will be smallest.

3) A small value of the magnetostriction in the preferred direction is favourable for squareness. Square-loop ferrites suitable for practical purposes, however, can be obtained only if the two first conditions are fulfilled. In the mixed-crystal systems referred to in figs. 5 and 6 this is not the case.

The frequency characteristics of the ferrite are also important. It is clear from the article I that a low value of μ_i will be accompanied by a high ferromagnetic resonance frequency: this is a primary requirement if the hysteresis loop is to be rectangular with pulses of about 1μ sec. It is also seen from I that it is just with those ferrites which have the smallest initial permeability that the irreversible Bloch-wall displacements are able to follow the current variations up to the highest frequencies. If difficulties due to eddy currents are to be avoided, moreover, the resistivity of the material must be sufficiently high. It appears to be not difficult to attain values higher than 10^2 or even 10^4 ohm metres (M.K.S. system), which means a factor of 10^9 to 10^{11} higher than that of metallic soft magnetic materials.

Examples of ferrites with rectangular hysteresis loops

Measurements of the hysteresis loop have been carried out with a ballistic galvanometer. The dependence of the results on the frequency will not be discussed here. Before considering the square loop materials, a brief review of some well-known materials will be given.

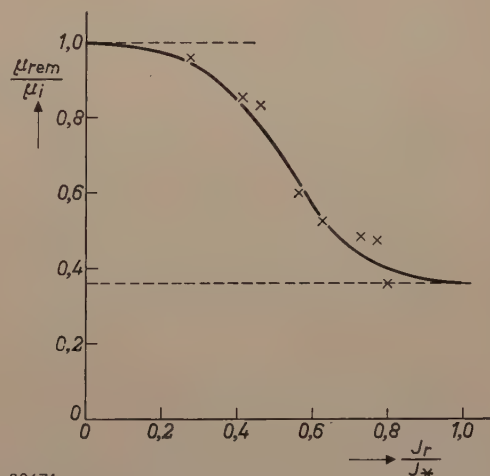
The porosity of Ferroxcube IIIB is about 10%. The coercive force and the crystal anisotropy are both low, and it can therefore be expected that the porosity will result in a considerably reduced value of J_r/J_* ¹⁵; in fact, an average value of 0.27 is obtained. Accordingly $\mu_{rem}/\mu_i = 0.96$. The squareness ratio is of course very small: $(R_s)_{max} \approx 0$.

Ferroxcube IVE has a higher coercive force ($\mu_0 H_c = 14 \times 10^{-4} \text{ Wb/m}^2$) and a larger crystal anisotropy (μ_i is only 17), both factors being favourable for a rectangular hysteresis loop. If this

material is fired at the normal temperature, however, it is very porous ($p = 25\%$), and the demagnetizing fields again become significant. It is found that $J_r/J_* < 0.6$; $\mu_{rem}/\mu_i = 0.63$, and $(R_s)_{max} = -0.15$. These values show an improvement when the material is fired at a higher temperature; the porosity is then only 10%. In this case, notwithstanding a decrease in coercive force (down to $\mu_0 H_c = 3 \times 10^{-4} \text{ Wb/m}^2$), the loop is more rectangular, viz. $J_r/J_* = 0.6$, $\mu_{rem}/\mu_i = 0.55$, and $(R_s)_{max} = 0.70$.

The chemical compositions and properties of a number of ferrites giving rectangular hysteresis loops, together with those of some other ferrites, are given in Table II. The relationship in sintered ferrites between μ_{rem}/μ_i and J_r/J_* can be seen from the table and from fig. 9. For low values of J_r/J_* , μ_{rem}/μ_i approximates to 1. For the maximum value that can be anticipated, viz. $J_r/J_* = 0.87$, the ratio μ_{rem}/μ_i should approach a value of 0.36, and this is roughly the case as shown in fig. 9. Striking results were obtained from the following ferrites.

1) $\text{Co}_{0.02}\text{Mn}_{0.48}\text{Fe}_2\text{O}_4$. The hysteresis loop of this ferrite is not particularly square, but the material has that advantage of a small coercive force: $\mu_0 H_c = 0.43 \times 10^{-4} \text{ Wb/m}^2$.



80674

Fig. 9. Relationship between the quantities μ_{rem}/μ_i and J_r/J_* .

2) $\text{CuO}_{0.1}(\text{MnO}_{1+\delta})_{1.1}\text{Fe}_2\text{O}_3$ is remarkable for its low coercive force: $\mu_0 H_c = 0.67 \times 10^{-4} \text{ Wb/m}^2$.

3) $\text{MgO}_{0.5}(\text{MnO}_{1+\delta})_{0.875}\text{Fe}_2\text{O}_3$ is a very close-grained ferrite. Some idea of the porosity can be obtained from the photomicrograph of the polished surface shown in fig. 10a. For comparison fig. 10b shows a similar photograph of the porous Ferroxcube IIIA ($p=9\%$). From the table it is seen that $(R_s)_{max} = 0.81$, whilst $(J_0/J_{Hm})_{max} = 0.96$.

4) $\text{Mn}_{0.1}\text{Ni}_{0.5}\text{Mg}_{0.4}\text{Fe}_2\text{O}_4$. Porosity 5%. This ferrite has remarkably good characteristics, viz.

¹⁵ By J_* is meant the magnetization of a ring measured at $\mu_0 H = 0.01 \text{ Wb/m}^2$ ($H = \text{oersted}$). Since H_c is very much smaller, an adequate approximation to J_s is obtained by replacing it by the slightly smaller value J_* .

Table II. Properties of ferrites with rectangular hysteresis loops.

No.	Chemical composition	Porosity <i>p</i> %	μ_i	μ_{rem}/μ_i	J_r/J_s	$(J_0/J_{Hm})_{max}$	$(R_s)_{max}$	$\frac{\mu_0 H_c}{H_c : oersted} :$ 10^{-4} Wb/m^2	$\frac{\mu_0 H_m}{(R_s)_{max}} \text{ for}$ 10^{-4} Wb/m^2
	Ferroxcube IIIB	10	1230	0.96	0.27	0.32	~0	0.8	
	Ferroxcube IVE,								
	fired at 1250 °C	25	17	0.63	<0.6	0.70	-0.15	14	
	" " 1450 °C	10	42	0.55	0.6		0.70	3	
1	$\text{Co}_{0.02}\text{Mn}_{0.48}\text{Fe}_2\text{O}_4$	6	83	0.86	0.41	0.83	0.59	0.43	0.48
2	$(\text{CuO})_{0.1}(\text{MnO}_{1+\delta})_{1.1}\text{Fe}_2\text{O}_3$	3	86	0.56	0.60	0.93	0.76	0.67	0.85
3	$(\text{MgO})_{0.5}(\text{MnO}_{1+\delta})_{0.875}\text{Fe}_2\text{O}_3$		55	0.49	0.73	0.96	0.81		1.35
4	$\text{Mn}_{0.1}\text{Ni}_{0.5}\text{Mg}_{0.4}\text{Fe}_2\text{O}_4$	5	138	0.48	0.76	0.95	0.83		1.7
5	$\text{Mg}_{0.4}\text{Ni}_{0.6}\text{Fe}_2\text{O}_4$		28	0.53	0.62	0.94	0.84		2.6
6	$\text{Li}_{0.46}\text{Ni}_{0.08}\text{Fe}_{2.40}\text{O}_4$	5	40	0.36	0.8		0.78		4.3
7	$\text{Li}_{0.25}\text{Cu}_{0.5}\text{Fe}_{2.25}\text{O}_4$	4					0.75		

$(J_0/J_{Hm})_{max} = 0.95$ and $(R_s)_{max} = 0.83$ with a field $\mu_0 H_m = 1.7 \times 10^{-4} \text{ Wb/m}^2$.

5) $\text{Mg}_{0.4}\text{Ni}_{0.6}\text{Fe}_2\text{O}_4$. The outstanding feature of this ferrite is that the squareness ratio is only very slightly dependent on the temperature. We shall return to this point later. It is found among the mixed crystals of Mg ferrite with Ni ferrite, that firing at 1450 °C does not always ensure low porosity; now and then a rectangular loop is obtained with $p = 20\%$. Microscopic examination of the polished surface gives the explanation: the high porosity is in this case due to much larger pores than in other ferrites. The initial permeability is low ($\mu_i = 28$).

6) $\text{Li}_{0.46}\text{Ni}_{0.08}\text{Fe}_{2.40}\text{O}_4$. It appears that "lithium ferrite" ($\text{Li}_{0.5}\text{Fe}_{2.5}\text{O}_4$) fired at 1000 °C in oxygen exhibits slightly negative magnetostriction. If it is chemically reduced by firing at a somewhat higher temperature (1150°C) so that a mixed crystal of lithium ferrite and ferrous ferrite is produced, a positive magnetostriction in the pre-

ferred direction is obtained. Intermediate firing temperatures, give the greatest squareness but it is still insufficient for practical purposes because the relatively low temperature results in too much porosity. Firing at higher temperatures gives a lower porosity, but an increased ferrous ferrite content, and hence not a low magnetostriction. An improvement was obtained by starting with a mixed crystal of lithium and nickel ferrite. The apparent density of this material is 4.60, and the actual density of the material itself is 4.85. This, combined with a high value of $|K|$ (since $\mu_i = 40$) promotes squareness of the loop (see Table II).

7) $\text{Li}_{0.25}\text{Cu}_{0.5}\text{Fe}_{2.25}\text{O}_4$. Porosity 4%, $(R_s)_{max} = 0.75$.

As explained above, the squareness ratio R_s of a hysteresis loop is a function of the maximum field strength H_m at which the loop is measured. Fig. 11 shows R_s as a function of H_m for the ferrites listed in Table II. It is seen that the lower the field strength

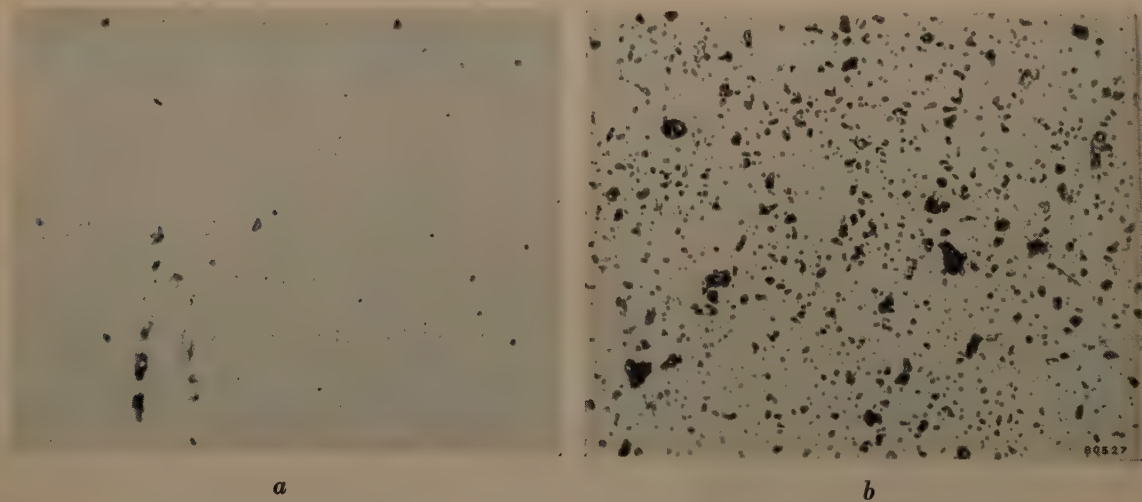


Fig. 10. Photo-micrographs of polished surfaces (magn. 400 ×). a) Ferrite No. 3 (Table II). b) Ferroxcube IVA. $p = 0.09$.

at which R_s reaches a maximum, the more R_s depends on H_m . The figure also shows the ratio J_0/J_{H_m} plotted against H_m . It may be noted that the optimum field for R_s is practically the same as for J_0/J_{H_m} .

Special properties

In many applications of square hysteresis loop ferrites a low temperature coefficient and high stability of the constants $(R_s)_{\max}$ and $(J_0/J_{H_m})_{\max}$

(except 40°C) a loop can be obtained which is more rectangular, corresponding to a different value of H_m , but it is found that the spread in $(R_s)_{\max}$ within a certain range of temperatures is smallest for those loops which refer to the optimum field H_m for the average temperature (40°C) in the working range.

Stability of the hysteresis loop

Fig. 13 shows an ideal rectangular hysteresis

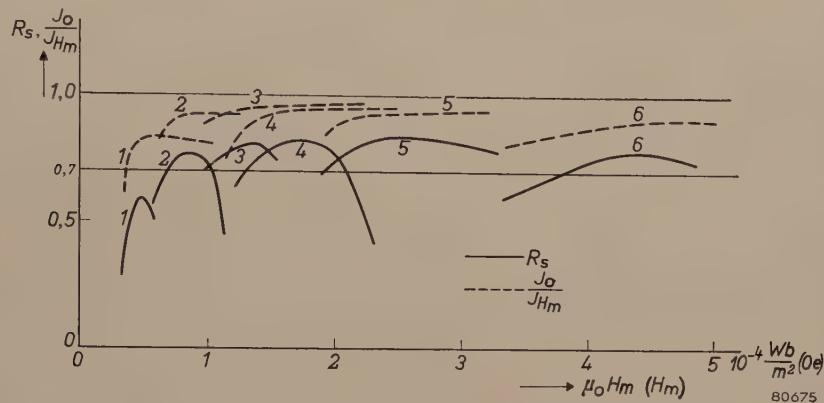


Fig. 11. R_s and J_0/J_{H_m} plotted against H_m for a number of the ferrites in Table II.

are also required. These factors will now be briefly reviewed.

Effect of temperature on $(R_s)_{\max}$

Different meanings can be attached to the dependence of $(R_s)_{\max}$ upon the temperature. We choose a temperature range of 20 to 60°C. in which R_s is determined in respect of values of H_m such that R_s at 40°C is equal to $(R_s)_{\max}$. The values obtained for a number of ferrites are plotted in fig. 12 against the temperature. At any temperature

loop. It will be clear that if this loop be followed round a number of times to the point where $H = H_m$, this will be the point I in the diagram. When H is made zero, point II will be reached. A current pulse which causes H to drop to $-\frac{1}{2}H_m$ brings us to point III and, if H then again becomes zero, the material will return to the state represented by point II. In the applications for which this material is employed the cycle II-III-II may

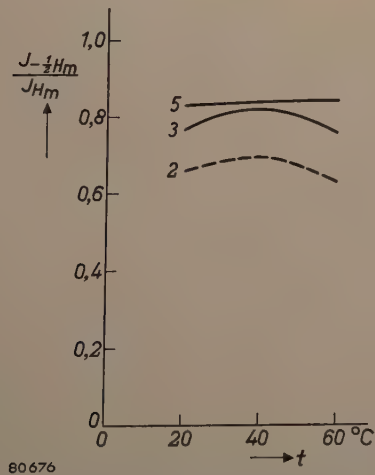


Fig. 12. R_s as a function of the temperature, for the three ferrites (2), (3) and (5) in Table II.

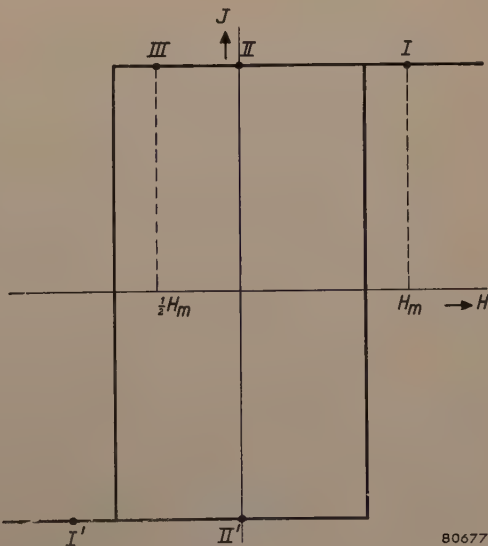


Fig. 13. Ideal rectangular hysteresis loop.

occur many times before a pulse of magnitude $-H_m$ arrives to bring the material into condition I' and then II' , i.e. to reverse the sign of the magnetization.

How far the non-ideal available materials approximate to this behaviour may be gathered from fig. 14. This shows one half of the hysteresis loop corresponding to the optimum squareness ratio for one quality of ferrite. The point I was measured after the field H_m had gone through a number of

cycles. When H_m is removed the point II is reached. An opposing field $-\frac{1}{2}H_m$ gives point III and, when this in turn is removed, a point IV is reached which is lower than II . The variation of points $I - IV$ when the cycle $I-II-III-IV$ is completed a number of times has also been investigated. Ferrite No. 2 in Table II was used for this purpose. It was found that after a large number of cycles of the subsidiary loop $I-II-III-IV$, the induction at point I had dropped by less than 1%. Point II remained constant within experimental error; point III rose: the corresponding induction value may increase by more than 5%. Point IV also rose considerably. The final situation is that the subsidiary loop has moved to the position shown by the broken line in fig. 14. Clearly, the squareness ratio R_s does not diminish but even increases, in this case from 0.76 to 0.81.

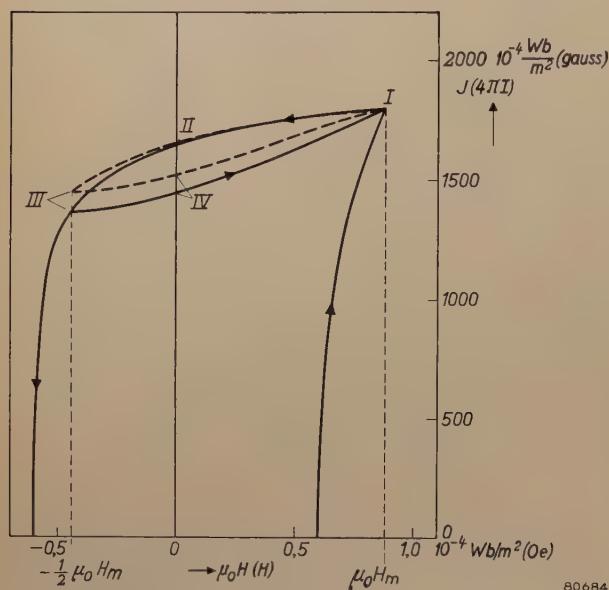


Fig. 14. Hysteresis loop of ferrite No. 2 (see Table II) when the field is varied a number of times from $H = H_m$ to $H = -\frac{1}{2}H_m$.

Summary. For certain purposes (computing machines, switching elements) cores of magnetically soft material (i.e. with small coercive force) are required, having almost rectangular hysteresis loops. Ferrites fulfil these requirements and also have the advantage that eddy currents and other losses are only small when the field is varied rapidly. The shape of the hysteresis loop of ferrites is determined by the nature of the anisotropy governing the direction of the magnetization vector (crystal, stress or shape anisotropy). Pronounced crystal anisotropy is an advantage (and with it the accompanying low initial permeability μ_i), but it should not be so high that the coercive force becomes too great. In order to minimize the other kinds of anisotropy, internal strain and porosity should be avoided. A number of suitable ferrites especially developed for the purposes mentioned above are described and their properties enumerated.

MIRROR CAMERAS FOR GENERAL X-RAY DIAGNOSTICS

by W. HONDIUS BOLDINGH.

778.33:771.31:616-073.75

The use of fluorography is becoming more and more common and is now also employed in general X-ray diagnostics. Attempts to minimize the dosage to which the patient is exposed during this type of examination have developed along two quite separate lines, namely, the improvement of optical efficiency in photographic systems, and the use of electronic aids (e.g. the X-ray image intensifier) to increase the image luminance. It is difficult at the present stage to predict the ultimate relationship between the two methods; the former, however, has now attained a considerable measure of perfection. The present article describes some of the latest designs of the fluorographic cameras used.

Fluorography, that is, the photographing of fluorescent X-ray images with the aid of a camera instead of by direct contact with a film, was originally developed for mass chest survey. The merits of the method as applied to this particular branch of diagnostics have been discussed fully in earlier issues of this Review^{1) 2)}. All that we need

recall here is that documentation is thus achieved without undue expense of film and filing space, and

- 1) A. Bouwers and G. C. E. Burger, X-ray photography with the camera, Philips tech. Rev. 5, 258-263, 1940.
- 2) H. J. di Giovanni, W. Kes and K. Lowitzsch, A transportable X-ray apparatus for mass chest survey, Philips tech. Rev. 10, 105-113, 1948/1949.

that a well-organised routine has been evolved during the examination of entire population groups.

The principal problem associated with the introduction of fluorography was the speed of the camera required to photograph the faint image on the fluorescent screen with a very short exposure. Lens cameras were initially used for fluorography but a considerable improvement was effected by introducing mirror cameras. Such a camera, based on the Schmidt optical system, and designed for 45 mm film, has been described earlier in this Review ³⁾ ⁴⁾. This camera, subsequently modified to some extent, can make almost distortion-free photographs of a flat fluorescent screen of (effective) area 42×42 cm, reduced in size by a factor $r \approx 10.5$. It contains an optical system with a mirror of 166 mm diameter and a correcting plate ⁵⁾ of diameter (D) 125 mm. The focal length f of the system is 104 mm. The effective aperture ratio (see the article referred to in ⁴⁾) of the camera at the above reduction factor is $1:N_{\text{eff}} = 1 : 1.03$. To compute this quantity (which is a true measure of the light-gathering power, see article referred to in note ⁴⁾), use is made of the formula:

$$1 : N_{\text{eff}} = \frac{D}{f} \frac{r}{r-1} \sqrt{S}$$

where S is the transmission of the optical system (otherwise termed the shadow factor): $1 - S$ indicates what fraction of the light proceeding towards the mirror is intercepted by the film holder.

The above-mentioned camera is provided with a wide range of attachments for automatic and foolproof operation in mass chest surveys.

Two more cameras of a similar type have recently been developed for use with 35 mm and 70 mm films, primarily because these sizes have been either standardized or recommended in several countries. In principle, the mirror optical system is the same in all three cameras (the 70 mm model is an enlarged version of the 45 mm camera scaled-up approximately proportionally to the ratio of the film sizes). Moreover, the film transport mechanism and the accessories of the two new cameras are not fundamentally different from the earlier camera; no further description is therefore necessary in this article.

³⁾ P. M. van Alphen and H. Rinia, Projection-television receiver, I. The optical system for the projection, Philips tech. Rev. **10**, 69-78, 1948/1949.

⁴⁾ W. Hondius Boldingh, Fluorography with the aid of a mirror system, Philips tech. Rev. **13**, 269-281, 1951/1952.

⁵⁾ Special consideration has been given to the diameter of the correcting plate. In practice the particular diameter adopted produces the optimum combination of light-gathering power and picture definition.

However, developments of another kind were taking place during the course of the work on the new cameras for mass chest survey, viz. the development of cameras for general diagnostics. The continued increase in the use of X-rays for general diagnostics has led to the desire to use fluorography also in this field. In some large hospitals the number of such examinations may mean over 1000 radio-graphs per day, the usual size, using contact radio-graphy, being 30×40 cm; hence the use of fluorography for even a portion of the daily examinations can mean an appreciable saving in the use of film. The application of fluorography to this field has become practicable as a direct result of the introduction of the mirror camera, which permits of a shortening of the exposure and consequently gives photographs of improved quality, suitable for many diagnostic purposes. This possibility was anticipated in the previous article ⁴⁾.

Certain requirements for mass chest survey, e.g. simplicity of operation and the positive identification of photographs, apply perhaps less stringently to a camera for general diagnostics; greater emphasis however, must now be placed on the picture-quality. Moreover, the equipment must be adapted to suit the methods of general diagnostic examination. With this in view, three new cameras have been designed, one for single exposures, one for a series of up to 30 photographs, and one for a similar series at high speed; these will now be described.

Picture-size of the new cameras

Each of the mirror cameras for general diagnostics is designed to take 70 mm film, this being so economical as compared with the full-size contact picture that there is virtually no incentive to adopt a smaller size. The special merit of 70 mm film is that in many cases of general diagnostics the relevant details can be seen direct from the film without enlargement, and that a critical examination of the photograph can be accomplished quite well with a simple optical aid such as a magnifying glass. The relatively greater weight and volume as compared with cameras for smaller film-sizes is not inconvenient in this application, which does not involve transportation. It is in fact generally recognized that 70 mm is the most appropriate film-size for this purpose.

The actual picture is of course narrower than the film, which is masked on either side by the film gate against which it is pressed during the exposure. The strips of film thus obscured are wider than in cameras used for ordinary photography, since with

the Schmidt mirror optical system it is necessary to give a spherical curvature to the film: a not too narrow margin is required to give adequate purchase on the film during the process of spherical deformation. Hence the picture-width of the 70 mm film for camera chest examination was limited to 58 mm (reduction factor 7.2). This figure has also been adopted in the new cameras, now to be described; the optical systems of all these 70 mm cameras are therefore identical.

Single exposure camera

As will be seen from *fig. 1*, the design of the single exposure camera is relatively simple. To position the film (flat film, cut to size 70×70 mm) between the concave mirror and the correcting plate a sliding cassette is used; in this the film is moulded to the required spherical shape by spherical pressure plate (*fig. 2*). The axial tolerance of the position of the film, or, more precisely, of the position of the centre of curvature of the spherical film-surface, is extremely critical: owing to the unusually high aperture-ratio of this camera, the depth of focus is so minute that a film displacement of only a few

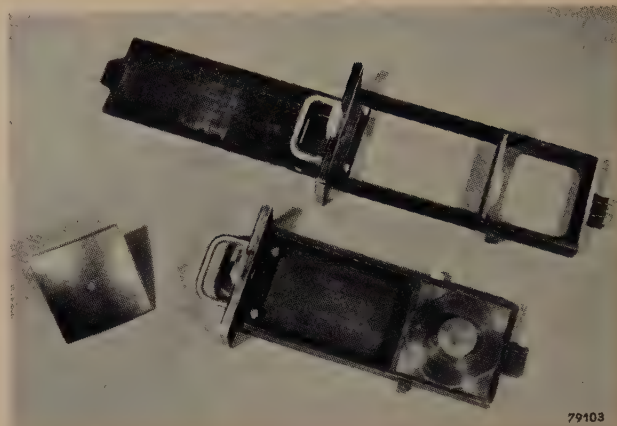


Fig. 2. A cassette (foreground) with the spherical pressure plate inserted; note the three lugs provided to ensure accurate centering. Above, the cassette with the spherical pressure plate (left) removed and the cassette cover withdrawn.

tens of microns is enough to produce a perceptible decrease in definition. The problem of attaining so high a standard of precision in the positioning of the film cassette could of course be solved by employing an extremely accurate finishing process for the cassette slide, but in view of the inevitable wear on the sliding faces, and to ensure reproducibility of position when changing the cassette, another method was adopted. Each cassette is provided with three lugs (*fig. 2*) whose surfaces facing the correcting plate form a continuation of the convex film surface or, more accurately, of the contact frame around the film gate. When the cassette has been inserted, it can be moved towards the correcting plate by turning a lever, until the three cassette lugs rest against the points of three set screws rigidly fixed with respect to the optical components (*fig. 3*). Since a spherical surface of a given radius (and direction) of curvature is uniquely located by three fixed points, precise positioning of the film is ensured.

The loss of light in this camera is smaller than in the other mirror cameras mentioned above, owing to the fact that cut film is used: no light-tight film-guide is therefore required between the gate and the outside of the camera, and when the cassette cover is withdrawn to expose the sensitized film surface, the optical system is substantially free of obstruction save for the film itself in the centre. Thus the transmission in this camera is very high, viz. $S = 0.79$, as compared with 0.49 in the 70 mm camera for mass chest survey, 0.55 in the 70 mm serial camera and 0.53 in the 45 and 35 mm chest survey cameras. The present instrument thus has by far the highest light-gathering power, its effective aperture ratio being $1 : 0.80$ as compared with 0.96, 1.0, 1.03 and 1.05 respectively for the other types referred to. The exposures required for this camera

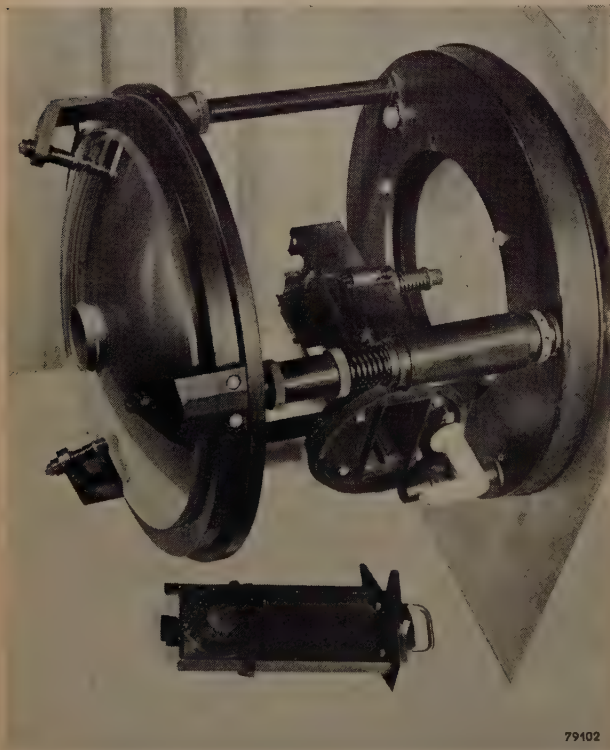


Fig. 1. Mirror camera for single exposures, with cover removed. (For the purposes of the photograph the camera is screwed to a wooden mount.) The concave mirror is on the left, and the correcting plate on the right of the photograph: between them is the cassette holder with slot for inserting the cassette, and a crank for pressing the cassette against the centering screws. A cassette is shown beneath the camera.

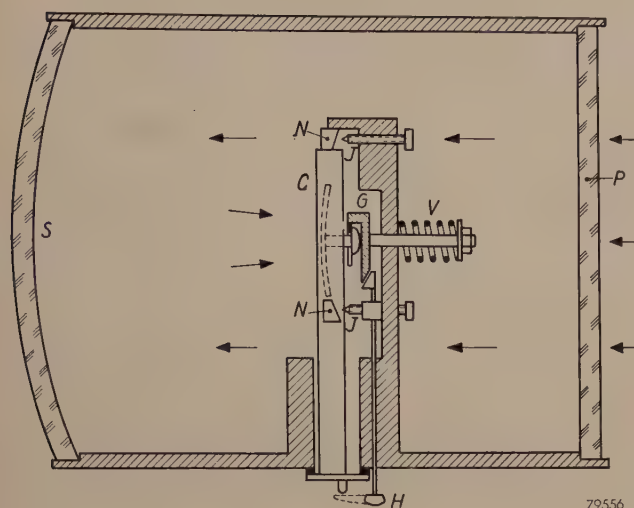


Fig. 3. Diagram illustrating the centering of the film. When the cassette *C* is inserted, the knob of the spherical pressure plate (fig. 2) engages with a bracket *G*. When the crank *H* is rotated a cam bearing on the bracket *G* allows the latter and hence also the cassette to be pulled to the right by spring *V* until the lugs *N* of the cassette rest upon the points of the set screws *J*. *S* is the concave mirror; *P* is the correcting plate.

are only about three times longer than those necessary for contact photographs, assuming the same voltage and current on the X-ray tube; they can of course be shortened considerably by in-

creasing the voltage on the X-ray tube. The consequent loss of contrast may be largely off-set by the use of a film with a higher gamma.

Camera for serial exposures

The serial camera (fig. 4) is designed for use in cases where frequent X-ray examinations are to be made so that it is not convenient to change the cassette before each exposure. The film is transported from a dispenser cassette capable of accommodating 30 m of film (enough for 400 photographs) to the film gate, and from there to a receiver-cassette capable of storing up to 30 photographs. When this total is reached, or sooner if desired (if necessary immediately after each individual exposure), the film can be cut off and the receiver-cassette removed from the camera to develop the exposed strip of film.

This camera is so designed that the cutting-off of individual photographs can be done without wasting relatively long strips of film; this has been achieved by a special modification of the usual film transport. Normally the film is *drawn* through the camera and over the spherical pressure plate,

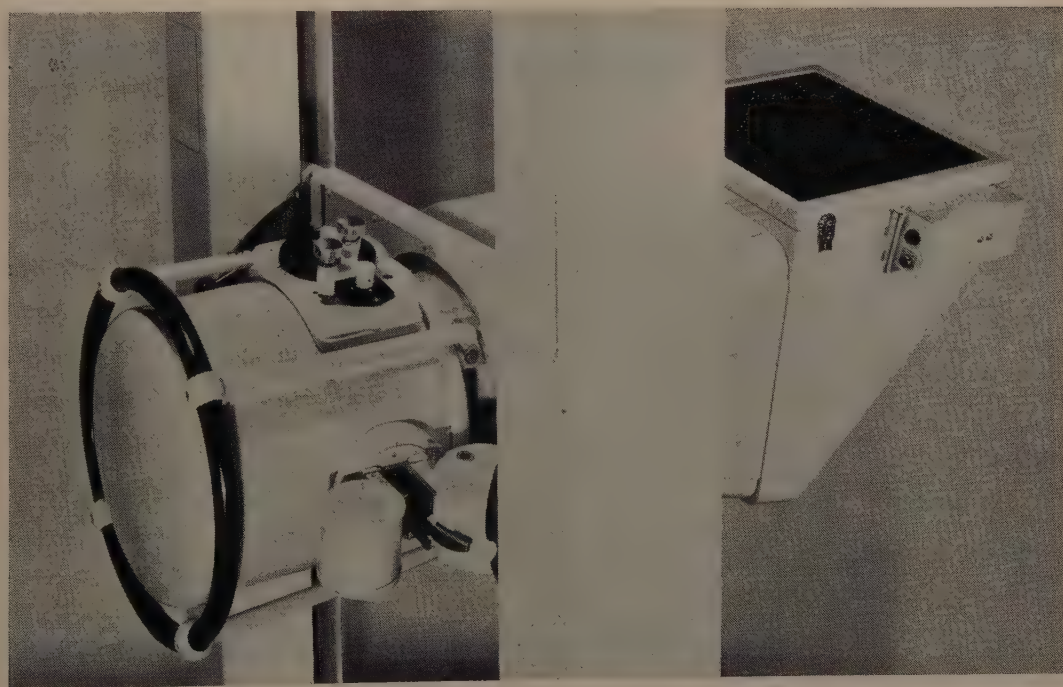


Fig. 4. Mirror camera for a series of up to 30 photographs. The dispenser cassette for 400 photographs (30 m of film) and the receiver-cassette are seen at the side of the camera; the film transport lever and the exposure counter, and another lever for film cutting are at the top of the camera. The camera is secured to an angular hood which slides up and down on vertical rails: the other end carries the fluorescent screen and a plane mirror set at an angle of 45° to the screen. The hood and camera can be rotated through approximately 270° about the axis of the camera so that, for example, photographs of a patient lying on an ordinary examination table can be taken vertically upwards or downwards.

by a traction wheel outside the optical system. The film cannot, of course, be severed between the traction wheel and the film gate, since the wheel could then exercise no pull on the film. To develop a photograph immediately after exposure (that is, without waiting until a number of other photographs has been taken), the portion of film concerned must therefore be advanced beyond the traction mechanism, leaving several picture-lengths unexposed.

In the serial camera, this is avoided by *pushing* instead of pulling the film strip past the gate. This permits the strip of film exposed and fed forward to be cut off very close to the film gate (fig. 5); only $2 \times \frac{1}{2} = 1$ picture-length per cut need then be spoiled (this being necessary to ensure the complete exclusion of light from the film on either side of the cut); hence the loss per strip of film cut off is equivalent to only one photograph. When the film is wound forward after the next exposure it passes through a funnel-shaped guide into a new receiver-cassette, in the place of the one removed.

To operate the film transport of the camera, a crank is rotated one full turn by hand. This releases the film in the film gate, transports the film by one

frame and re-applies the spherical deformation to the film.

Although the optical system is the same as that of the single exposure camera described above and the mass chest survey camera, the three cameras differ so appreciably in other particulars of design that no attempt has been made to furnish them with identical or interchangeable components. Uniformity of this kind would merely make each type individually more complex and more expensive.

Serial camera with rapid film transport

"Functional" X-ray examination, whereby the motions of functioning organs are demonstrated, usually with the aid of a contrast agent introduced into the body, is an important branch of radiology. Such examinations often involve taking upwards of ten photographs in quick succession. The development of this valuable diagnostic technique using contact radiography has been hitherto impaired by the high cost of film and the difficulty of attaining the desired rapid succession of exposures.

With the introduction of fluorography conditions have become much more favourable for the development of this technique. It has been found possible to design a film transport mechanism for the serial camera operating at a speed that will produce 5 pictures per second. This rapid film movement is accomplished with the aid of an electro-mechanical drive operating in the manner demonstrated in fig. 6. An electric motor mounted on the camera,

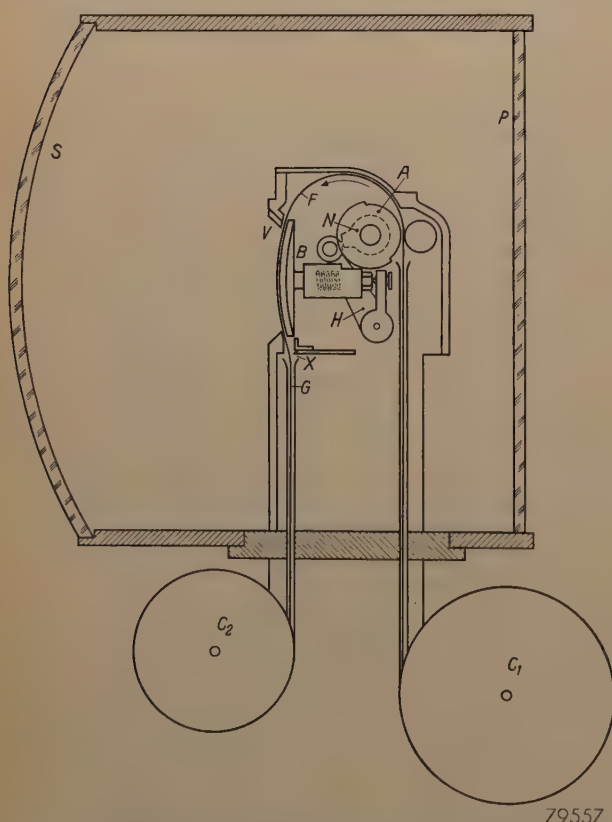


Fig. 5. Section (greatly simplified) of the camera for serial exposures. Note the friction roller *A* which actuates the spherical pressure plate *B* by means of a cam *N* and a lever *H* and aided by a pressure roller, pushes the film strip *F* past the film gate *V*. Also shown are the cutter at *X* and the funnel-shaped guide *G* to the receiver-cassette *C*₂, which receives the film as fed forward. *C*₁ is the dispenser-cassette.

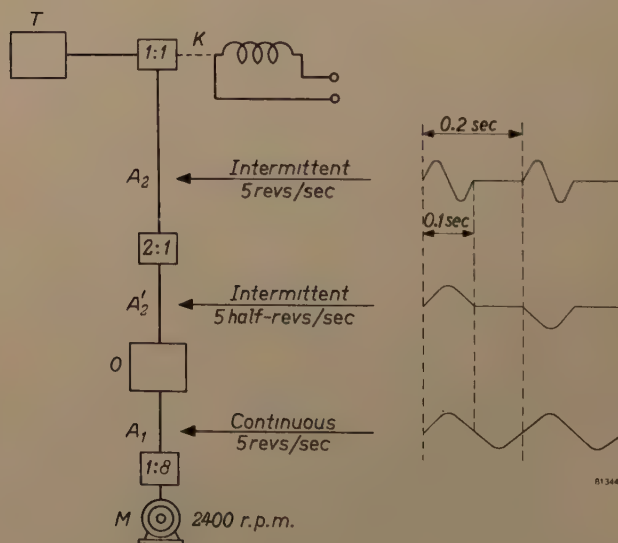


Fig. 6. Schematic diagram of the film transport mechanism of the rapid sequence serial camera. The revolutions of the continuously rotating spindle *A*₁ and of the intermittently rotating spindles *A*₂' and *A*₂ are shown schematically on the right. *M* motor, *O* feed-mechanism, *K* electromagnetic clutch, *T* film transport and actuating mechanism for pressure plate. As long as *K* is engaged, the film is advanced 5 times per second and a photograph (exposure not exceeding 0.1 sec) is taken after each advance.

drives a spindle at a speed of 5 revolutions per second (A_1), which actuates a feed-mechanism (O). This in turn drives another spindle (A_2) intermittently, so that it rotates one full turn in $\frac{1}{10}$ second, remains stationary for a similar period, then executes another full turn, and so on. This intermittently rotating spindle can be coupled by means of an electromagnetic clutch to the film-transport drive, which is otherwise identical with that of the serial camera already described. When this clutch is engaged (during a stationary period) the next revolution of A_2 causes a complete cycle of the film transport, that is, the retraction of the spherical pressure plate, the feeding forward of the film and the spherical deformation of the next frame of film. During the subsequent stationary period of A_2 , which lasts $\frac{1}{10}$ of a second, a fluorogram can be recorded; for this purpose a contact in the camera transmits an electric signal to the time switch of the X-ray apparatus. At the end of the stationary period, the spindle again rotates, the film is fed forward, and so on.

It will be seen that as long as the magnetic clutch remains engaged, 5 photographs per second will be recorded, each with an exposure not exceeding $\frac{1}{10}$ second (the time switch of the X-ray apparatus is of course pre-set to give the desired exposure). The electromagnetic coupling, however, between

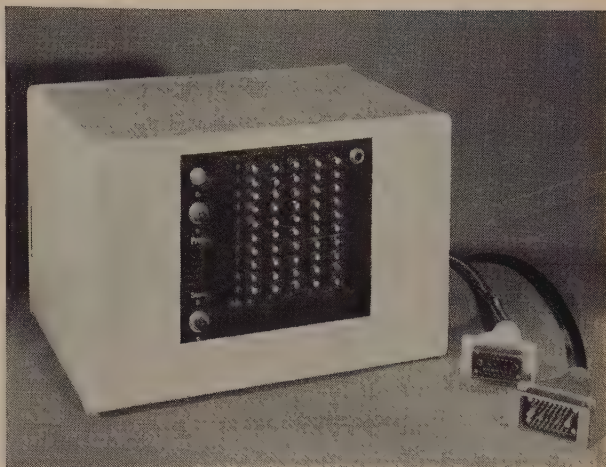


Fig. 7. Programme selector for camera with high-speed film transport. The 50 press-buttons correspond to the 50 periods of $\frac{1}{5}$ second occurring within 10 seconds. Whether or not the magnetic clutch is to be engaged, i.e. whether or not a photograph is to be taken in any particular period is determined in advance by means of the appropriate button.

the intermittently rotating spindle A_2 and the film transport can be interrupted at will for one or more periods after the forward movement of the film, so that fewer photographs are taken per second (if necessary with exposures exceeding $\frac{1}{10}$ second). This is accomplished with the aid of a specially designed accessory known as the programme selector (fig. 7), containing a series of 50 contact knobs

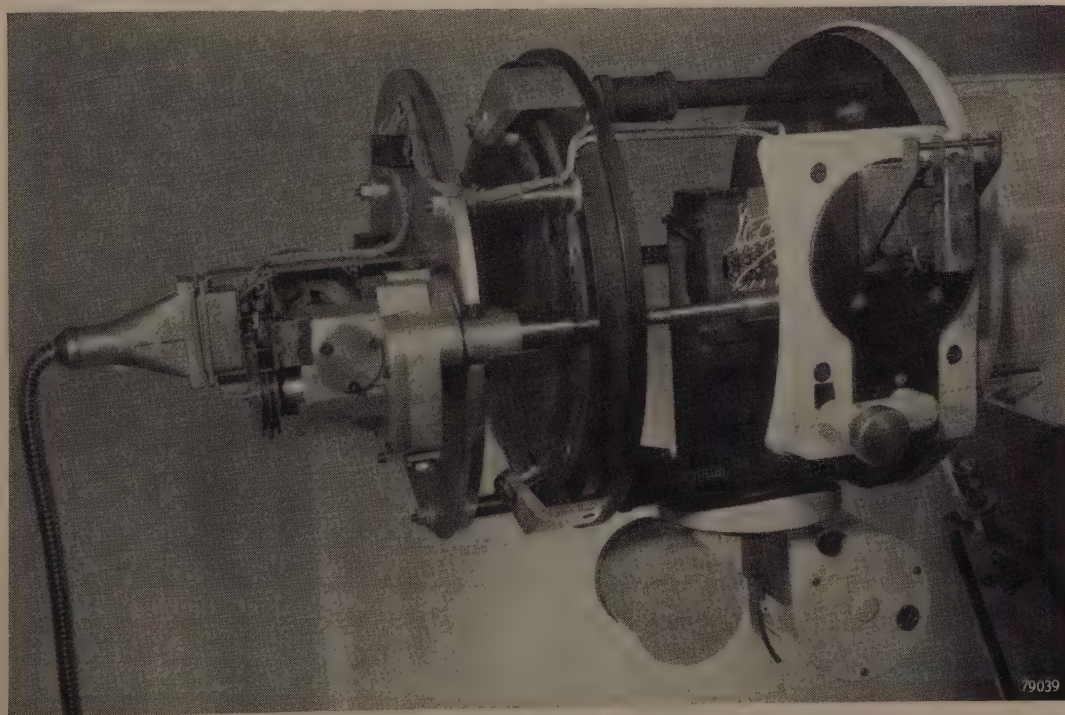


Fig. 8. Interior of mirror camera with high speed film transport. The feed mechanism is seen on the left, and behind it the electric driving motor; on the right is the electromagnetic clutch which couples the intermittent spindle (A_2 in fig. 6) to the actual film transport at the predetermined intervals

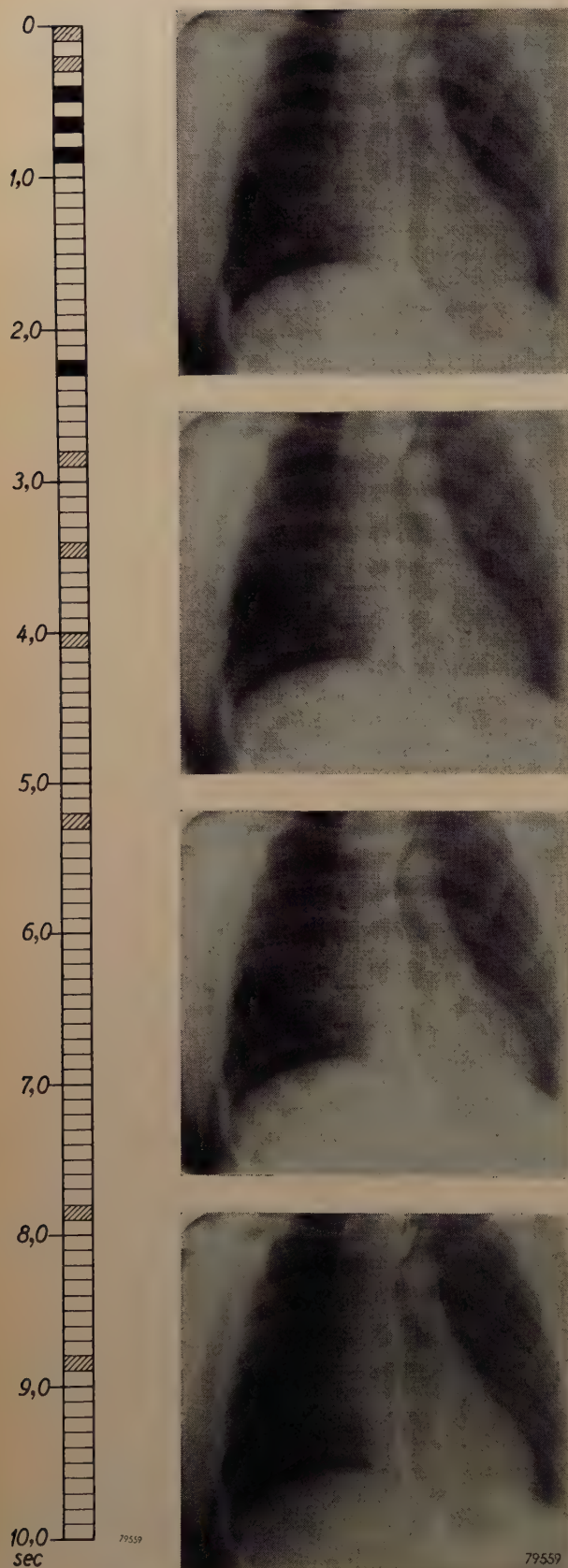


Fig. 9. Four photographs of the oesophagus taken with the rapid sequence mirror camera. The scheme of the whole series is seen on the left; hatched areas indicate periods in which photographs were taken; the four blackened areas correspond to those reproduced here. The contrast agent administered enables the act of swallowing to be followed.

corresponding to the 50 revolutions (cycles) performed by the intermittently rotating spindle in 10 seconds. Before every series of exposures, the magnetic coupling for each period is pre-set through a system of relays by means of the appropriate knob, that is, it is possible to determine beforehand whether or not the film shall be advanced and the X-ray apparatus switched on during a particular period. In this way it is possible to map out the whole scheme of photographs before exposure.

The feed-mechanism (driven by the continuous spindle A_1), which governs the intermittent rotation of spindle A_2 , is a counterpart of the well-known Maltese-cross mechanism used in film projectors⁶). The Maltese cross mechanism of the type most commonly used, rotates $\frac{1}{4}$ turn in a quarter period of the driving shaft and then remains stationary for the remaining three-quarters of the period. In our system, which is based on a picture-period of $\frac{1}{5}$ second, the above time-ratio would leave only $\frac{1}{40}$ second for the actual film transport (another $\frac{1}{40}$ second being required for the spherical deformation of the film). This involves a film acceleration so high as to involve a serious risk of damage to the film. For this reason a new mechanism with a feed period equal to the stationary period was designed to supply the intermittent movement required. The intermittent spindle A_2 of this mechanism performs one half revolution in the first $\frac{1}{2}$ cycle of the continuous spindle A_1 , and remains stationary during the remainder of that cycle. A 2:1 gear coupling A'_2 to A_2 produces in the latter (which carries the friction wheel of the film transport) a rotation through one full turn. This gear-up is necessary because if the friction wheel were carried on the shaft A'_2 ($\frac{1}{2}$ turn per cycle of operations) the diameter necessary to transport the film with the picture-size adopted would be inconveniently large.

A photograph of the high-speed camera with covers removed is shown in fig. 8.

As an example of the results obtainable with the high-speed camera, fig. 9 shows a series of photographs taken during a functional diagnostic examination of the oesophagus. The rate at which the contrast agent (or an air-bubble contained in it) descends through the oesophagus during the act of swallowing can be ascertained by comparing these photographs. A good deal of the clarity is

⁶) A description is given in an article by J. J. Kotte on a professional 16 mm film projector, to be published shortly in this Review.

necessarily lost in the half-tone reproduction but the quality of the original photographs is in every way sufficient for such an examination.

Summary. Fluorography, originally developed for mass chest surveys, is now also becoming important in general X-ray diagnostics. Three Schmidt type mirror cameras designed for this purpose, each using 70 mm film and having a reduction

factor of 7.2, are described. The first, of effective aperture ratio 1 : 0.80, is for single exposures. The method of film-centering in this camera is described in detail. The second camera, which is fitted with dispensing and receiving cassettes, can take a series of up to 30 photographs, but the film can be cut off and developed after only one or more exposures. The film wastage is minimized by pushing, instead of pulling the film through the film gate. The last of the three, largely identical with the serial camera just mentioned, has a high-speed film transport which permits 5 photographs to be taken per second, a valuable feature for functional radiography.

ABSTRACTS OF RECENT SCIENTIFIC PUBLICATIONS OF N.V. PHILIPS' GLOEILAMPENFABRIEKEN

Reprints of these papers not marked with an asterisk * can be obtained free of charge upon application to the Philips Electrical Ltd., Century House, Shaftesbury Avenue, London W.C. 2.

2078: W. K. Westmijze: Gap-length formula in magnetic recording (*Acustica* 2, 292, 1952).

A formula is derived for the dependence of the frequency characteristic of a magnetic reproducing head on the gap-length.

2079: H. G. van Bueren: On the attraction between a perfectly conducting plate and a thin perfectly conducting cylinder (*Proc. Kon. Akad. Wet. Amsterdam* B 55, 493-499, 1952, (No. 5).

By analogy with the formula of Casimir, $E = -(\pi^2/720)(h/2\pi)cL^2/R^3$, for the interaction between two parallel conducting plates of area L^2 , due to zeropoint energy, it is found that the interaction energy between a thin wire (radius r_0 , length L) and a square plate of area L^2 is

$$E = -(3/16) (h/2\pi) cr_0^2 L/R^4.$$

If $r_0 = 2\mu$ and $R = 5\mu$ the force of attraction is equal to that due to a potential difference of about 0.3 mV.

2080: H. Bruining: Quelques points de vue nouveaux concernant la construction et l'utilisation de l'image iconoscope (*Le Vide* 71, 1248-1255, 1952, No. 42). (Some new points of view regarding the construction and utilization of the image iconoscope: in French.)

In this article on the construction of an image-iconoscope, special attention is given to means of suppressing ion burn. This is achieved by placing a fine-mesh grid close to the photo-cathode, thus avoiding concentration of the ion beam. The advantage of using a L-cathode (diffusion cathode) in the electron gun is stressed. In addition, an electron lens system is described allowing a continuous change of the focal length of the camera. A special device is described for ensuring equality of brightness, especially at the boundary of the image field. See also Philips tech. Rev. 14, 327-335, 1952-53.

2081: B. D. H. Tellegen: Synthesis of four-poles (*Proc. Symp. Modern Network Synthesis*, New York N.Y., 1952, pp. 40-49, publ. by Polyt. Inst. Brooklyn N.Y.).

General considerations on the synthesis of four-poles with preconceived properties, by means of inductances, capacitances, resistances and ideal transformers. A fifth possible type of network element is the gyrator. See these abstracts, No. R73.

2082: J. L. Meijering: Calculs thermodynamiques concernant la nature des zones Guinier-Preston dans les alliages aluminium-cuivre (*Rev. Métall.* 49, 906-910, 1952). (Thermodynamical calculations concerning the Guinier-Preston zones in aluminium-copper alloys; in French).

According to calorimetric measurements on solid Al-Cu alloys by Oelsen and Middel the enthalpy of mixing is negative over the entire range of concentrations. This appears to be in contradiction to the current picture of the initial stages of precipitation hardening in aluminium with 5% Cu, which demands (when rather forced explanations are to be avoided) a segregation tendency in the face-centered cubic phase. Such a tendency is commonly due to a positive mixing-enthalpy curve. In this paper it is shown, by combining the calorimetric data with the solubility curve of Al_2Cu in Al, that the mixing-enthalpy curve is partly concave, partly convex, this making the contradictions disappear. Similar strongly asymmetric mixing-enthalpy curves must also appear in the systems Al-Ag and Pt-Ag.

2083: J. I. de Jong, J. de Jonge and H. A. K. Eden: The formation of trimethylol urea (*Rec. Trav. Chim. Pays-Bas* 72, 88-90, 1953).

In concentrated aqueous solution and in the presence of an excess of formaldehyde, more than two

methylo groups may be attached to one molecule of urea. The equilibrium constant of the formation of trimethylo urea is evaluated.

- 2084:** K. H. Klaassens and C. J. Schoot: Derivatives of p-diethoxybenzene, I. 1,4-diethoxy-2-chlorobenzene-5-diazonium-borofluoride (Rec. Trav. chim. Pays-Bas **72**, 91-93, 1953).

Description of the preparation of the above-named compound, and confirmation of its structure.

- 2085:** W. J. Oosterkamp: The radiography of the human body with radioactive isotopes (Brit. J. Radiology **26**, 111, 1953).

The activity of a number of radioactive isotopes, per mm² of surface of a layer of a thickness equal to one half-value layer (with a maximum of 10 mm), is compared to the emission, per mm² focus, of X-ray tubes (stationary and rotating anode). It is shown that the use of radioactive isotopes, even if short-lived and carrier-free, for medical radiography is only attractive for those applications where the use of X-ray tubes is not practicable.

- 2086*:** J. D. Fast and E. M. H. Lips: Metallurgical research in the Netherlands (Metal Progress **63**, 109-111, 1953).

Some practical results in the field of metallurgical research are enumerated, e.g. dies for deep drawing, blanking operations, drawability and brittleness of sheet metal, permanent magnets ("Ticonal" and "Ferroxdure"), gases and metals, hardening by internal oxidation, influence of admixtures on scaling rate, embrittlement of iron by oxygen, ageing, and welding with contact electrodes.

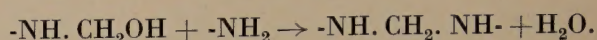
- 2087:** J. M. Stevels: Note on the ultraviolet transmission of glasses (Proc. 11th Int. Congress pure & appl. Chem. **5**, 519-522, 1953).

Considerations on the influence of bridge-oxygen ions and non-bridging oxygen ions on the ultraviolet absorption limit of glasses. Bridge oxygen shifts the absorption edge towards smaller wavelengths, non-bridging oxygen towards larger wavelengths.

- 2088:** J. I. de Jong and J. de Jonge: Kinetics of the formation of methylene linkages in solutions of urea and formaldehyde (Rec. Trav. chim. Pays-Bas **72**, 139-156, 1953).

A kinetic investigation is made of the reactions between monomethylo urea, dimethylo urea and urea in acid aqueous solution. Strong indications are obtained that these reactions are all of one

type, viz. bimolecular hydrogenion-catalyzed reactions between an amidomethylo group and an amide group, leading to the formation of methylene linkages between urea fragments:



The rate constant of this reaction appeared to depend on the type of amide group or amidomethylo group that is reacting. The activation energy is about 15 kcal/mole. The reaction between two molecules of dimethylo urea was found to be very slow if occurring at all. The possibility of cyclic structures arising from trimerisation of monomeric methylene urea and of the formation of dimethylene ether linkages between urea fragments may be excluded.

- R 206:** J. D. Fast and J. L. Meijering: Anelastic effects in iron containing vanadium and nitrogen (Philips Res. Rep. **8**, 1-20, 1953, No. 1).

The maximum quantity of nitrogen taken up by an iron wire containing 0.5 atomic % vanadium during heating at 950 °C in N₂ with 1% H₂, corresponds to one atom N per atom, plus a further amount of the same order as the quantity taken up by pure Fe under identical conditions. The first amount combines chemically with the vanadium and causes no internal friction. The extra quantity gives rise not only to a damping peak corresponding to that in pure iron (with an oscillation period of 1.3 seconds at 21.5 °C), but also to a peak at higher temperatures. This peak cannot be described with a single relaxation time only. It is due to the presence of (sub-microscopic) VN particles in the metal. These do not directly cause damping, but cause the free N-atoms to be bound much tighter in the surrounding interstitial sites than in the normal interstices. These abnormal interstices, therefore, will capture free N-atoms rapidly, whereupon the latter give rise to the abnormal damping. The binding energy in the abnormal interstices is not the same for all sites, and with coarsening of the VN precipitate the distribution of these energies is displaced in the direction of stronger binding. This is deduced from a shift of the summit of the second peak towards higher temperatures (from 80 °C to 88 °C in the authors' experiments) as the heating time at 950 °C is prolonged. From the intermediate state where they cause the abnormal damping, the N-atoms pass over rapidly into the fully precipitated state (iron nitride), where they cause no damping. Consequently, the VN precipitate exerts a strongly accelerating influence on the precipitation of dissolved nitrogen.

- R 207:** C. G. J. Jansen and R. Loosjes: The velocity distribution of electrons of thermionic emitters under pulsed operation, Part I, Apparatus and measuring technique (Philips Res. Rep. **8**, 21-34, 1953, No. 1).

This paper describes the construction of a tube for detecting the electron-velocity distribution of emitting surfaces, especially of oxide coatings at high current densities. With the apparatus used in conjunction with this tube it is possible to measure the electron velocities with an accuracy of about 1%. The i - V characteristic of the total emitting surface (8 mm²) and of the areas (0.03 mm²) whose velocity spectra are observed, can be determined with rectangular pulses or D.C. Complete i - V characteristics of the total emitting surface were also determined with pulses with a linearly sloping flank having a time interval of about 5 microseconds. Typical velocity spectra obtained from (BaSr)O, BaO and SrO coatings, and from the L-cathode (diffusion cathode) are shown. With tubes of similar construction equipped with an L-cathode, peak voltages can be determined with an accuracy of about 1 volt, independently of repetition frequency or pulse width.

- R 208:** H. C. Hamaker: The efficiency of sequential sampling for attributes, Part I. Theory (Philips Res. Rep. **8**, 35-46, 1953, No. 1).

In principle, Wald's probability-ratio sequential plans require three parameters for their specification. It is shown that for practical purposes we may with advantage use the two-parametric set of plans with decision lines symmetric with respect to the origin. There is no specific advantage in using an asymmetric position of the decision lines, while for the symmetric position the equations for sequential sampling can be greatly simplified.

- R 209:** J. W. A. Scholte and W. Ch. van Geel: Impedances of the electrolytic rectifier (Philips Res. Rep. **8**, 47-72, 1953, No. 1).

The system aluminium/aluminium oxide/electrolyte behaves as a rectifier. The conductivity of the layers out of which the oxide is composed changes with the externally applied potential difference. This article describes a method of deriving an electrical equivalent circuit of the oxide layer (consisting of a number of capacitors with resistors in parallel) from the frequency dependence of the impedance. The dependence of the state of the oxide layer on the D.C. potential across it is shown in a number of diagrams, in which the specific resistance is shown as a function of the

position in the oxide layer. All diagrams show a layer with a high resistance and a layer in which the resistance decreases sharply, followed by a layer of low resistance. With electric fields in the conducting direction, no permanent change of the oxide appears and only the resistance of the high-resistance layer varies with the applied voltage. In stronger electric fields which do cause a permanent change of the oxide layer, the highly conductive layer grows at the expense of the less conducting layer or vice versa. The electrical equivalent circuit is a starting point for discussion of the structure of the oxide layer. The conclusion is that both at the aluminium boundary and at the electrolyte boundary, the composition of the oxide shows a deviation from the simple stoichiometric ratio and is a semiconductor. It is assumed that rectification occurs by means of the contact between p-type and n-type semiconducting layers.

- R 210:** C. G. J. Jansen and R. Loosjes: Graphs for rapid calculation of the work function of thermionic emission (Philips Res. Rep. **8**, 81-90, 1953, No. 2).

These graphs are based on Richardson's formula, either in the form $j_s = A_0 T^2 \exp(-e\varphi/kT)$, or in the form $j_s = AT^2 \exp(-e\varphi_0/kT)$, where j_s is the saturation current density, φ the work function at temperature T , φ_0 the same at $T = 0$, e the electronic charge, k Boltzmann's constant, and $A_0 = 120$ A/cm². The latter form takes into account the dependence of φ on T , making the constant A differ from A_0 . The authors prefer the first form, however, from which φ can be derived at a given temperature. j_s is measured by a rapid oscillographic method. By computing φ for a number of temperatures it is possible to determine φ_0 and A , if desired. A number of graphs are added, making calculations unnecessary.

- R 211:** C. M. van der Burgt: Dynamical physical parameters of the magnetostrictive excitation of extensional and torsional vibrations in ferrites (Philips Res. Rep. **8**, 91-132, 1953, No. 2).

Tensile and torsional vibrations can be easily excited by magnetostriction in non-conducting ferromagnetics like ferrites. A simple experimental method permits rapid determination of the dynamic elastic and magnetoelastic constants, the complex nature of which is discussed after a comprehensive survey of the four sets of simultaneous magnetostriction equations of interest, under adiabatic conditions and under arbitrary depolarization. In reasonable agreement with the theory, the stress-

sensitivity constant and the magnetomechanical coupling coefficient of several Ni-Zn ferrites proved to be of the same order of magnitude as those of metallic magnetostrictive materials in common use. Moreover these ferrites (Ferroxcube IV materials) show much lower elastic dissipation at ultrasonic frequencies. Mechanical Q -factors up to 15 000 have been obtained at 50 kc/s. The variation of elastic and magnetic lag with frequency and biasing polarization is discussed. A considerable part of the total elastic losses at optimum bias consists in macro-magnetoelastic losses accompanying the macro-polarization induced magnetostrictively. The experimental correlation between the conductivity and the elastic and magnetic losses is explained in terms of elastically and magnetically excited micro strains that give rise to an electronic diffusion process. The order of magnitude of the molecular field is derived from the influence of the magneto-caloric effect on the magnetoelastic constants near saturation.

R 212: S. Duinker: An approximate graphical analysis of the steady-state response of non-linear networks (Philips Res. Rep. 8, 133-147, 1953, No. 2).

The steady-state response of essentially non-linear networks containing iron-cored inductors with simultaneous a.c. and d.c. magnetization is analysed by means of an approximate graphical procedure. It is shown, that under various conditions, jump phenomena (so-called ferro-resonance effects) may occur when circuit parameters (e.g., applied voltage, polarizing voltage, etc.) are varied gradually. Instabilities are found to exist in the series circuit consisting of a non-linear inductor, a linear capacitor and a small resistor when driven by a voltage generator, and also in the parallel circuit of the same elements but with a high value of the resistor and driven by a current generator. Three different kinds of jump phenomena can be distinguished depending on whether or not a jump corresponds to a transition from a capacitive to another capacitive state or from a capacitive to an inductive state or vice versa and, further, on the number of stable possibilities linked with the effect. It is pointed out that the analysis is not restricted to the special configuration of non-linear inductors considered but that it also applies to circuits containing capacitors and resistors with centro-symmetrical characteristics. The results arrived at may be of value in connection with the investigation of the influence of resistive and reactive loads of magnetic and dielectric amplifiers and the application of jump phenomena in ferro-resonant flip-flops.

R 213: W. K. Westmijze: Studies on magnetic recording, Part I (Philips Res. Rep. 8, 148-157, 1953, No. 2).

In this series of papers some problems are treated concerning the physics and mathematics of magnetic recording. In particular those problems are dealt with that arise in the recording of sound, where a strictly linear relationship between original and reproduced signals is required. This introduction gives a brief survey of the principle, some technical details and the history of magnetic recording. The mutual relation of the problems to be treated is explained.

R 214: W. K. Westmijze: Studies on magnetic recording, Part II (Philips Res. Rep. 8, 161-183, 1953, No. 3).

The magnetic field in front of the gap of some simple types of recording head is calculated as the solution of a two-dimensional potential problem. Applying the reciprocity principle the magnetic flux through the coil of a reproducing head, originating from a sinusoidally magnetized tape in front of the gap, is deduced. It is shown that the well-known gap-loss formula $(\sin 2\pi l/\lambda)/(2\pi l/\lambda)$, where l is the gap length and λ the wavelength on the tape) holds only in a theoretical case. A more general formula is given.

R 215: E. S. Rittner: A theoretical study of the chemistry of the oxide cathode (Philips Res. Rep. 8, 184-238, 1953, No. 3).

A comprehensive theoretical analysis of the chemistry of the oxide cathode, based upon thermochemistry and diffusion theory, is presented. The treatment is based on the conventional supposition that excess barium is required to activate the coating, and accordingly a search is made for materials of sufficient reducing power to serve as activators. Metals which fall into this category include: Th, Mg, Be, Hf, Sc, Y, Sm, Nd, Pr, La, Zr, U, Al, Si, C, and possibly Ti and Ce. A detailed analysis of the factors limiting the generation of free Ba reveals that the most favourable reaction mechanism is that in which the reaction speed is limited by the rate of diffusion of activator in the core metal. The free Ba subsequently finds its way into the individual oxide via the processes of Knudsen flow of the vapour and volume diffusion. An important requirement for the latter process is that the coating be constituted of a porous mass of fine particles. The paper concludes with a discussion of the evaporation loss during life of the excess Ba.